A1. Appendix A - Comparison of connection test results and predictions using component method

A1.1 Introduction

This appendix presents a complete set of results for the component-based methods and the respective experimental test data under both static and dynamic conditions. Some tests used a single loading ram to provoke a rotation whilst others used dual loading rams to provide direct axial loads and restrict rotation. The dimensions (Figure A1-1) were recorded prior to each test.

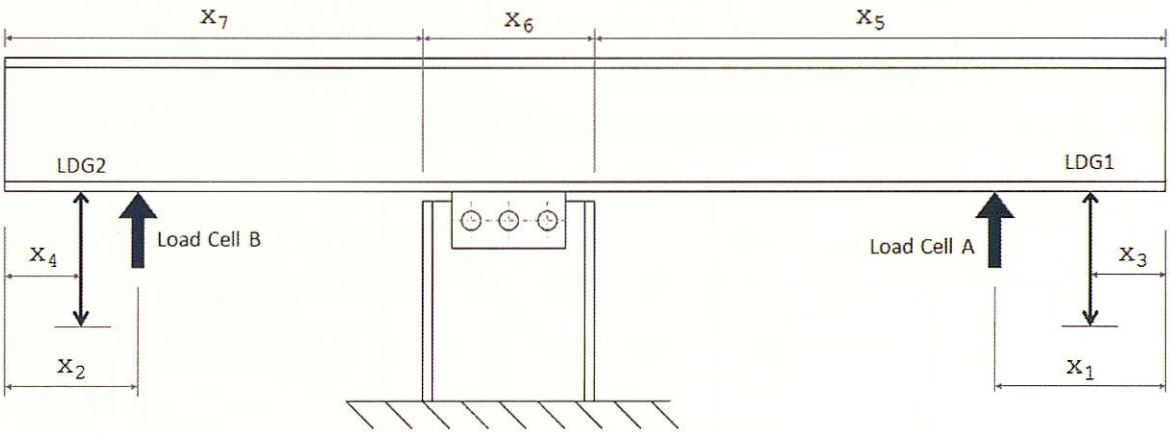

Figure A1-1: Test dimensions

For dynamic tests the physical movement of the column section is recorded and a comparison against the prediction using component-based methods shown. In addition the applied force/moment is plotted against the displacement/rotation. For static tests only the force/moment against displacement/rotation is presented as there was no need to display the time history analysis.

The dynamic tests are characterised by the diaphragm arrangement used to release the pressure within the system, where A is the weakest diaphragm arrangement and E the strongest. Hence a DYN (E) test is likely to have experienced a greater load than a DYN (A) test. The true load was recorded for each test.

A1.2 Fin plate connections

Test Number	Test Type	Loading Type	Failure
FIN1	Moment-rotation	Dyn (C)	Bolt in shear
FIN2	Moment-rotation	Static	Bolt in shear
FIN3	Direct tension	Static	Bolt in shear
FIN4	Direct Tension	Dyn (E)	No failure during the test but large bearing defamation of the beam web was observed
FIN5	Moment-rotation	Dyn (A)	Bolt in shear

A1.2.1 Fin plate connection test 1 (FIN1)

Dynamic test (1 thick and 1 thin diaphragm) with single loading ram.

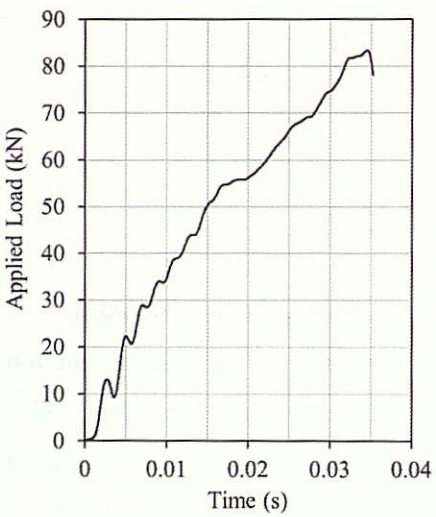

(a) Rotation-time

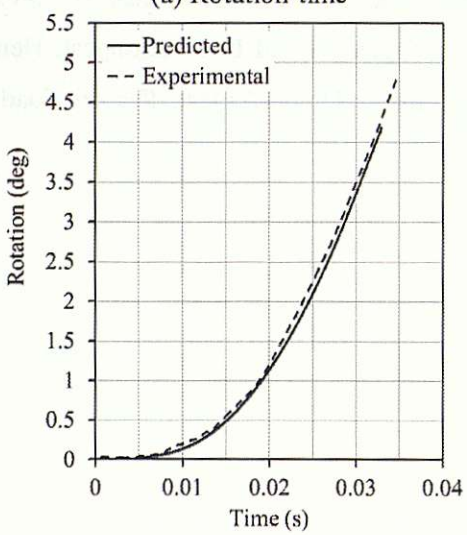

(b) Rotational velocity - time

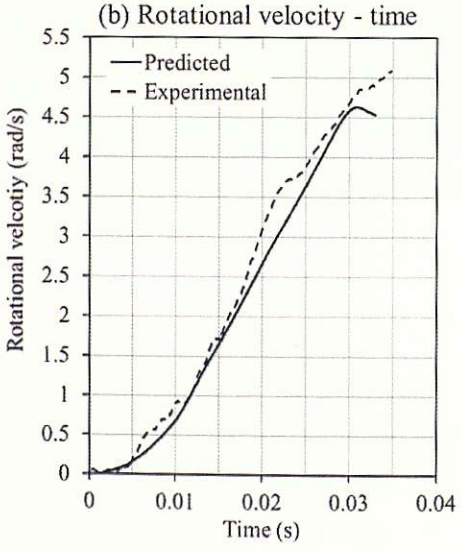

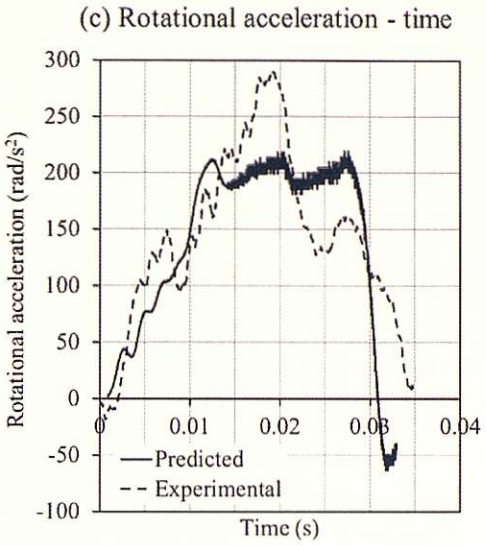

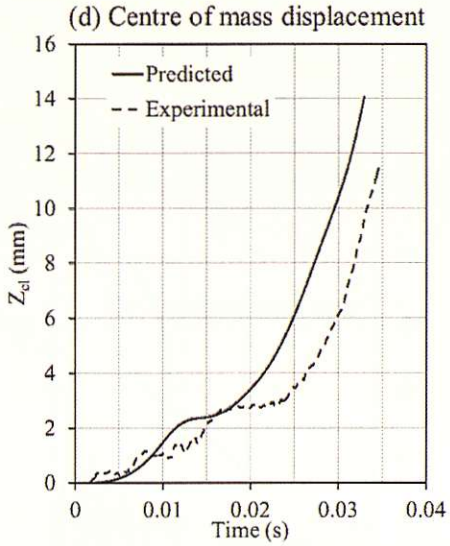

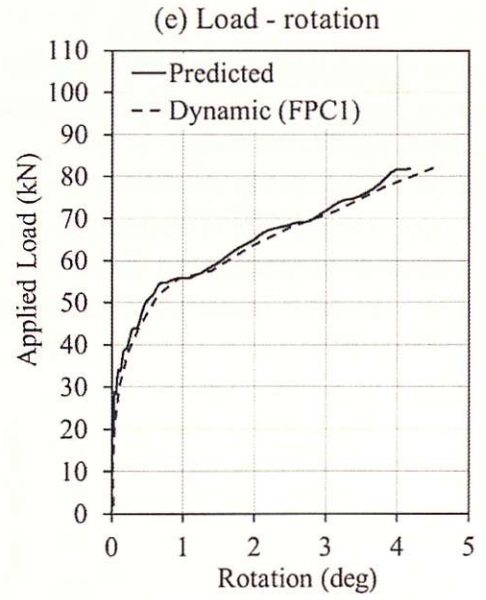

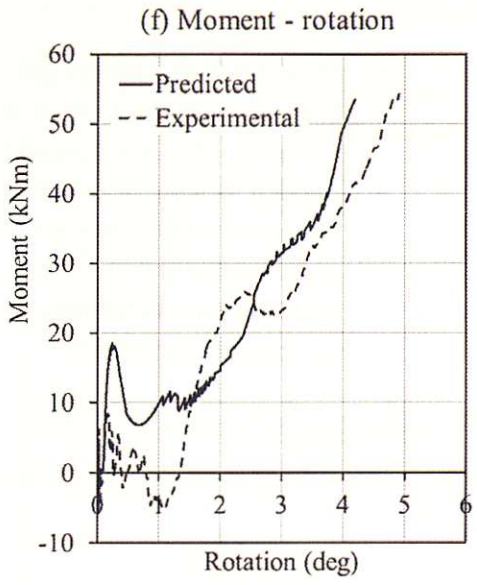

- Good correlation between predicted and experimental results for rotation of flying column
- Centre of mass displacement was over predicted
- Stiffness of connection from moment-rotation curve was predicted with reasonable accuracy
- Overestimation of ultimate moment capacity

A1.2.2 Fin plate connection test 2 (FIN2)

Static test with single loading ram.

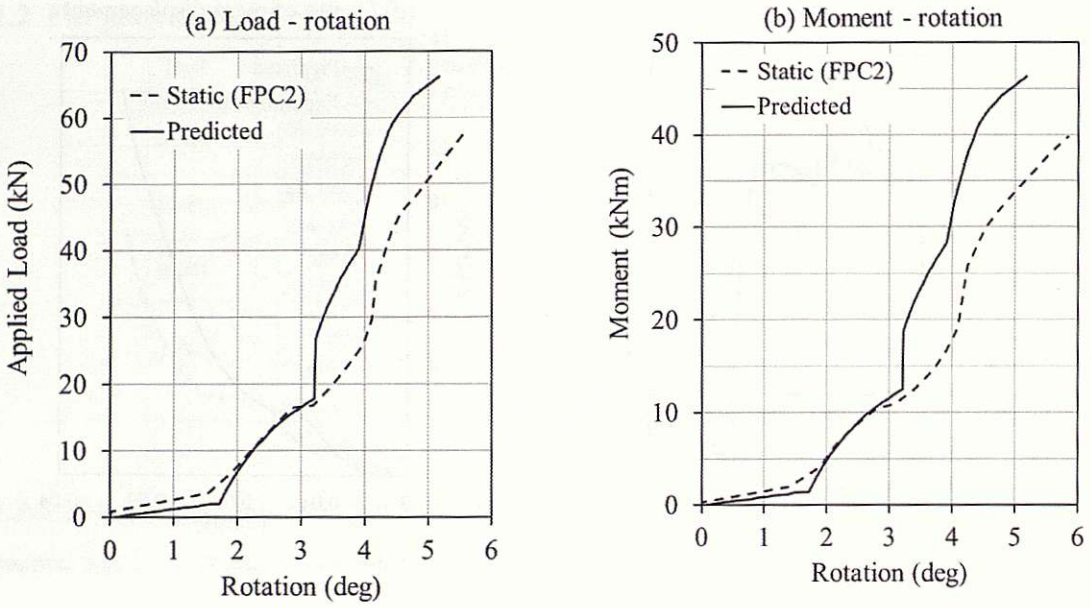

- Static prediction shows good correlation against the experimental test in the first phase up to a rotation of 3.2 degrees. Post yield stiffness is overestimated for specified rotation possibly due to crushing of beam flange
- Sudden increase in stiffness is a result of bearing against the column which changes the pivot location and thus results in an increase in moment. In the experimental test this occurs over a rotation of approximately 1 degree
- Failure rotation and moment capacity are reasonably accurate and within 5% of experimental values

A1.2.3 Fin plate connection test 3 (FIN3)

Static test with dual loading rams for direct tension testing.

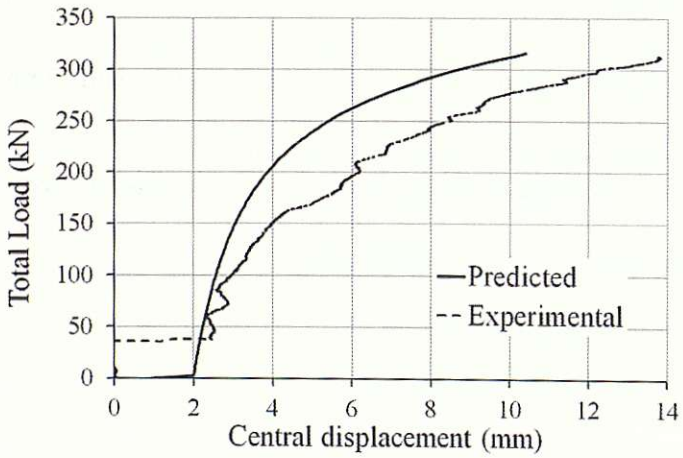

Figure 1-2: Load-displacement comparison (FPC3)

- Initial stiffness due to friction is not very accurate
- Increased stiffness when bolts begin to bear against the plate at 2mm displacement is captured

- General shape is predicted well but final displacement is off by approximately 3.5 mm which is reasonable considering the length of the column section is 2m

A1.2.4 Fin plate connection test 4 (FIN4)

Dynamic test (2 thick diaphragms) with dual loading rams for direct tension testing. The connection did not fail during the initial dynamic loading phase.

(a) Centre of mass - time

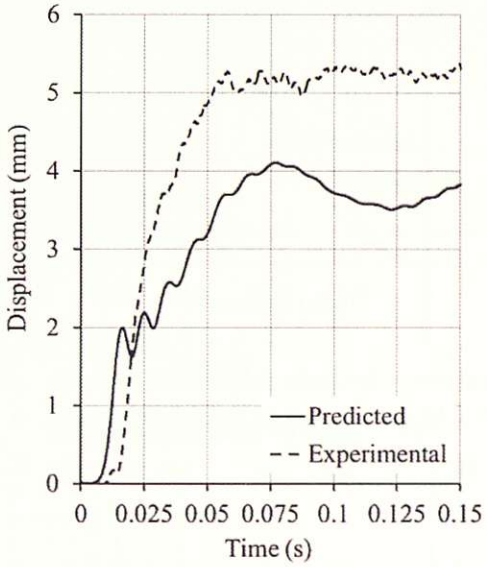

(b) Acceleration - time

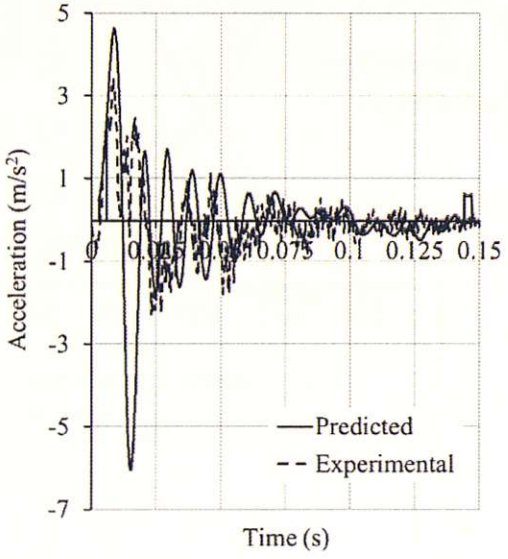

(c) Load - centre of mass displacement

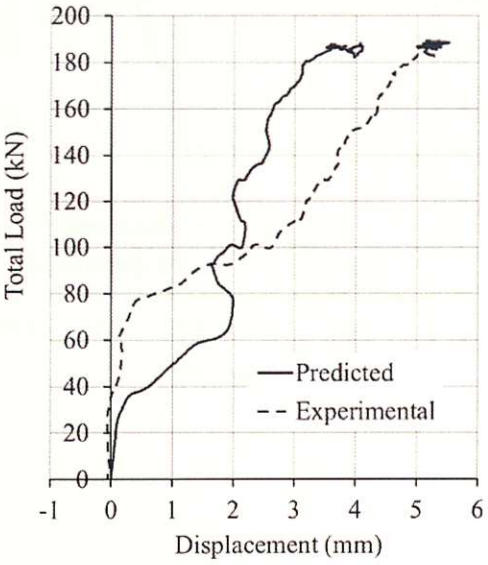

(d) Bolt group forces in component model

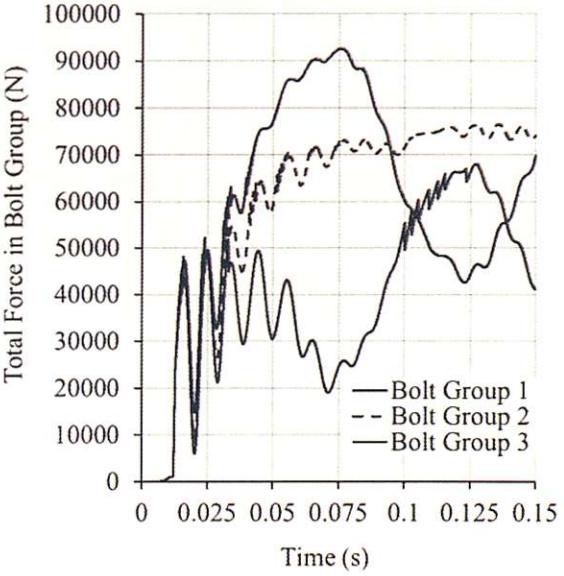

- No failure was predicted in agreement with the experimental result
- Difficult to test two rams dynamically because the pneumatic system meant slighty unequal loads were applied through the two rams leading to rotation and oscillations
- The unequal loads recorded in the test were input into the prediction model hence the resulting oscillations
- The experimental yield load appears to be approximately 60 kN compared to a predicted value of 40kN with final displacements of 5 and 4 mm respectively

A1.2.5 Fin plate connection test 5 (FIN5)

Dynamic test (2 thin diapragms) with a single loading ram.

(a) Rotation - time

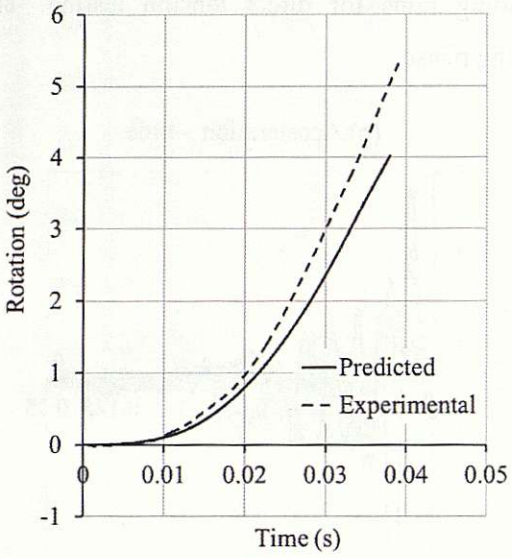

(b) Rotational velocity - time

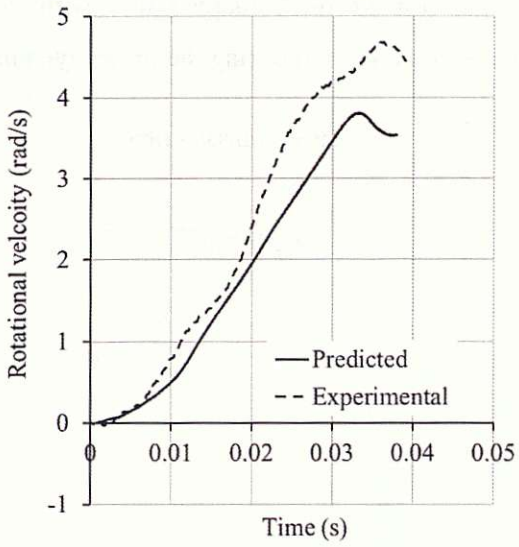

(c) Rotational acceleration - time

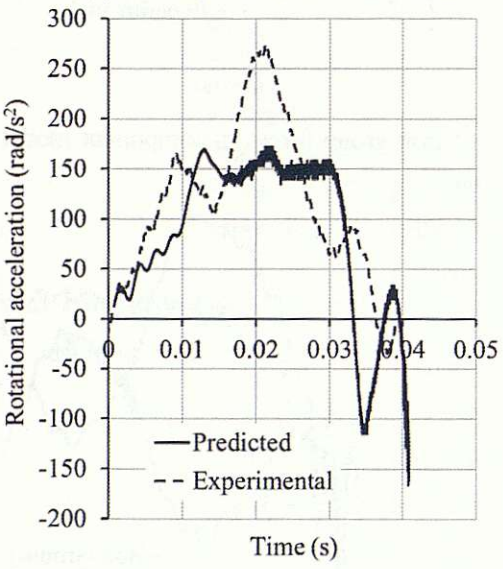

(d) Centre of mass displacement

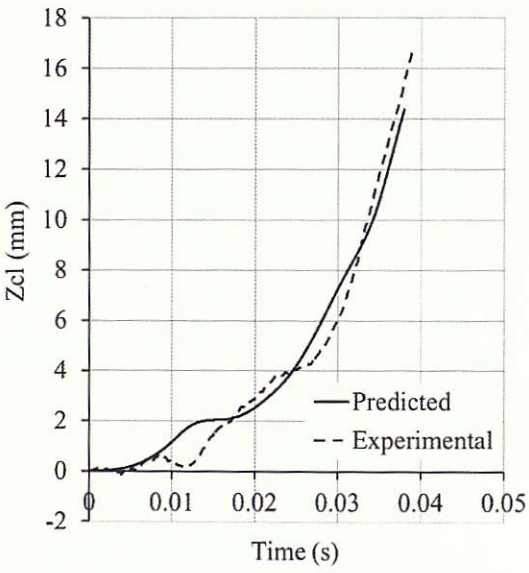

(e) Load - rotation

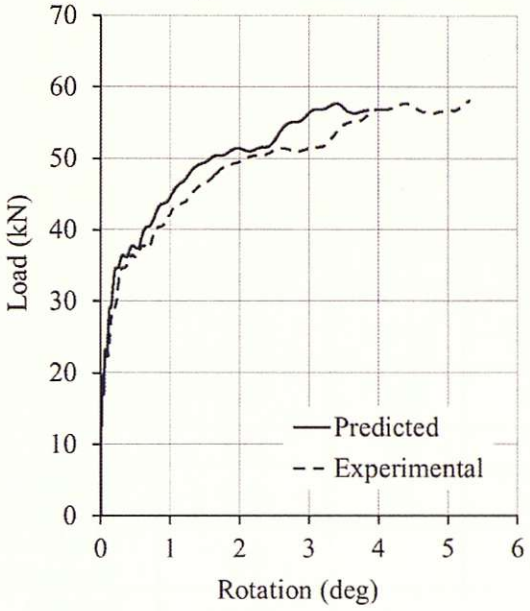

(f) Moment-rotation

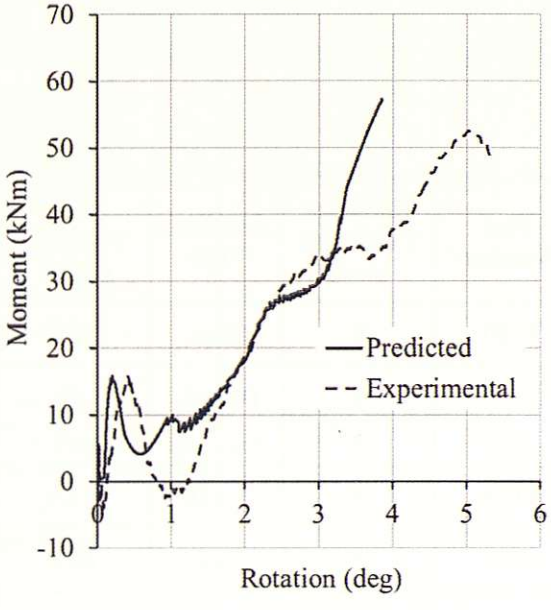

- General behaviour showed a good correlation with the experimental data
- Over prediction of the post yield stiffness and moment capacity

A1.3 8mm FLEXIBLE ENDPLATE CONNECTIONS

Test Number	Endplate Thickness (mm)	Loading Type	Peak Moment (kNm)	Failure Rotation (deg)	Peak Loading Time (ms)	Peak applied axial load (kN)	Failure
FEP1	8	Static	50.2	6.2	-	58.8	Endplate fracture
FEP2	8	Dyn (E)	75	5.8	40	97.7	Endplate fracture
FEP3	8	Dyn (A)	60.1	6.3	39	52.3	No
FEP4	8	Dyn (B)	63.4	5.8	40	65.7	Endplate fracture
FEP5	8	Static	48.3	6.7	-	56.8	Endplate fracture
FEP6	8	Dyn (E)	73.1	7.0	47	84.2	Endplate fracture
FEP9	8	Dyn (A)	54.8	-	40	47.4	No Failure
FEP9 (cont)	8	Static	45.7	7.4	-	54.2	Endplate fracture
FEP14	8	Dyn (A)	57.7	5.6	37	45.0	Endplate fracture
FEP16 (datalogger failed to trigger)	8	Dyn (A)	-	-	-	-	Yes (endplate)
FEP18	8	Static Tension	-	-	-	260.6	Endplate fracture
FEP19	8	Dyn (E) Tension	-	-	48	218.3	No Failure
FEP19 (cont)	8	Static Tension	-	-	-	281.1	Endplate fracture
FEP20	8	Dyn (E) Tension	-	-	53.2	157.7	No Failure
FEP20 (cont)	8	Static Tension	-	-	-	280.5	Endplate Fracture

A1.3.1 Flexible end-plate test 1 (FEP1)

8mm thick endplate

Static test with single loading ram

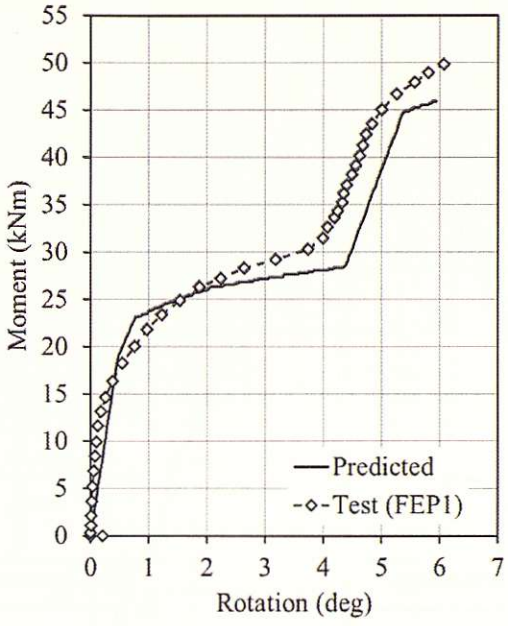

- Experimental elastic stiffness is higher than that predicted however the general trend shows a good correlation
- The point at which the beam flange contacts the column appears to be out by about ½ of a degree where the test data shows an increase in stiffness from about 4 degrees rotation
- The prediction model overestimates the failure rotation by nearly 3 degrees

A1.3.2 Flexible end-plate test 2 (FEP2)

8mm thick endplate

Dynamic test with single loading ram

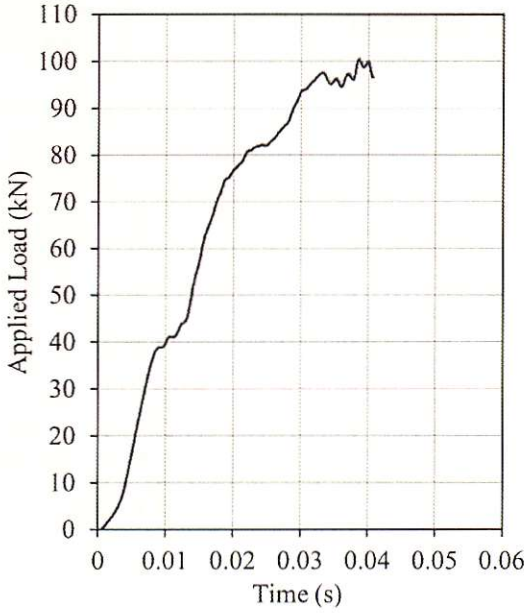

(a) Rotation-time

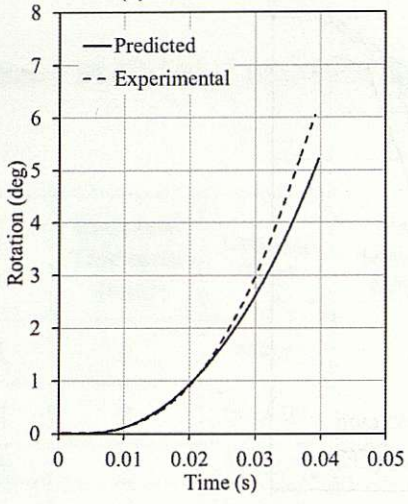

(b) Rotational velocity-time

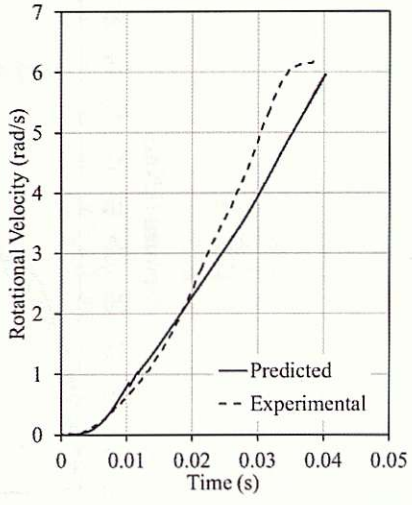

(c) Rotational acceleration-time

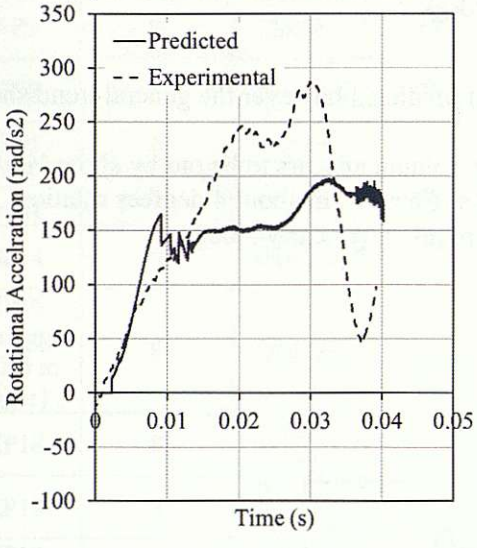

(d) Centre of mass displacement

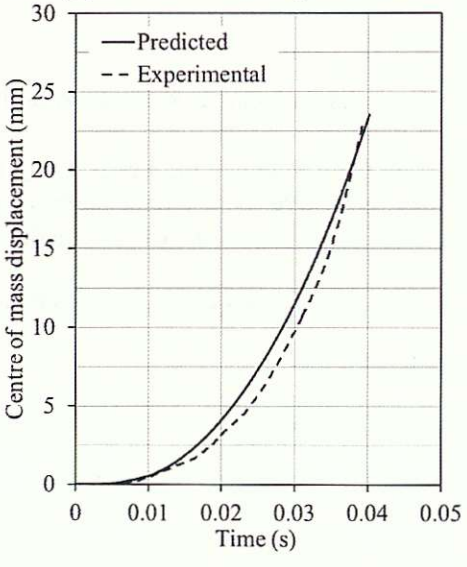

(e) Load-rotation

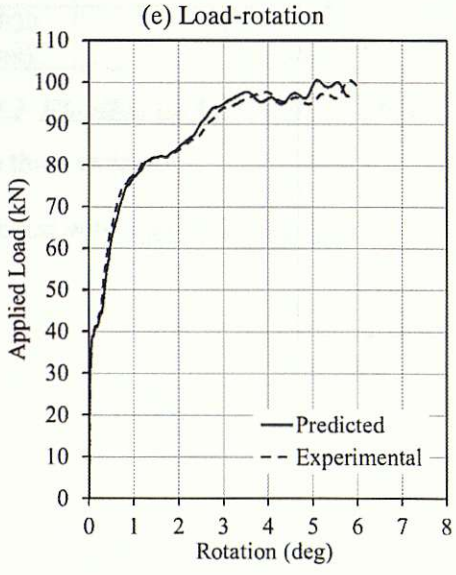

(f) Moment-rotation

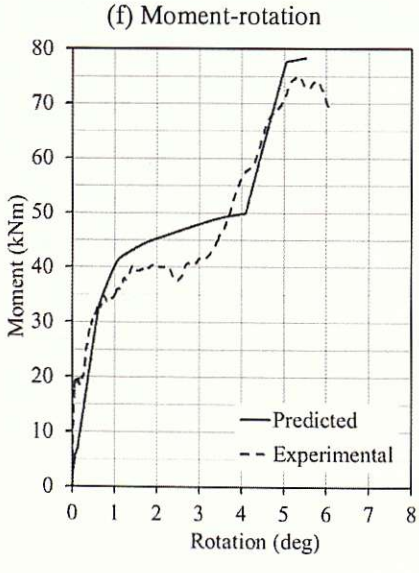

A1.3.3 Flexible end-plate test 4 (FEP4)

8mm thick endplate

Dynamic test with single loading ram

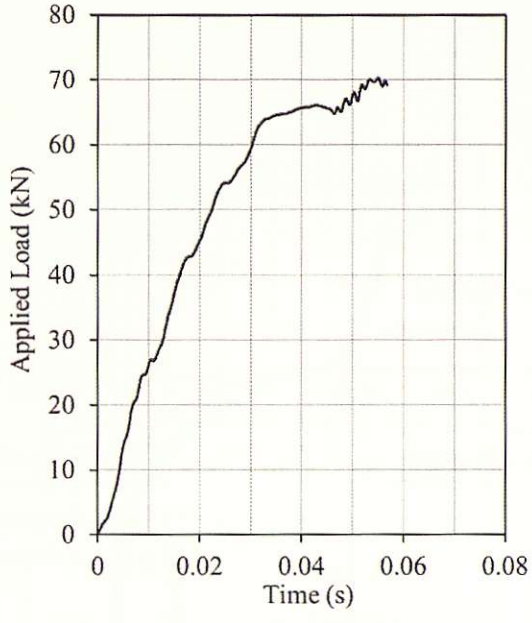

(a) Rotation-time

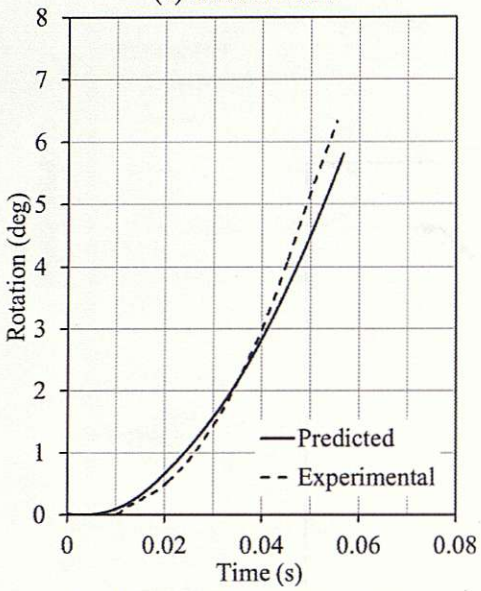

(b) Rotational velocity-time

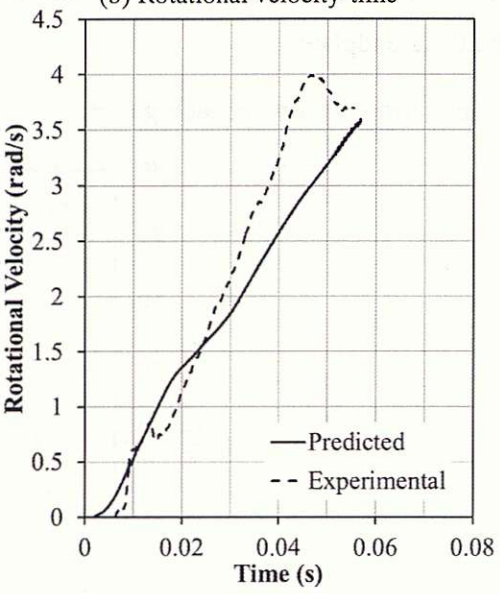

(c) Rotational acceleration-time

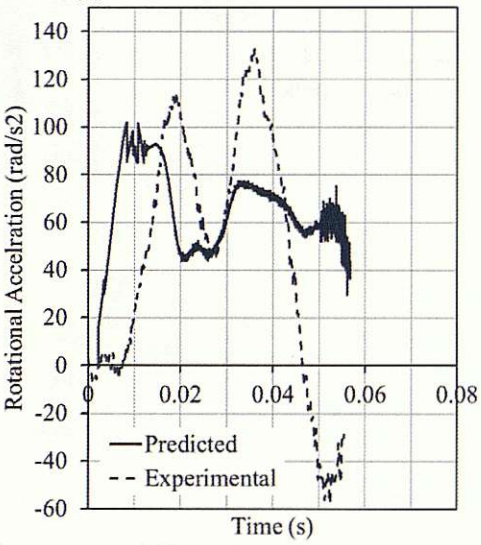

(d) Centre of mass displacement

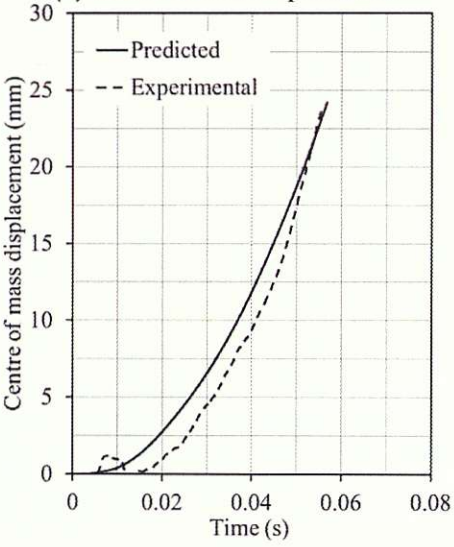

(e) Load-rotation

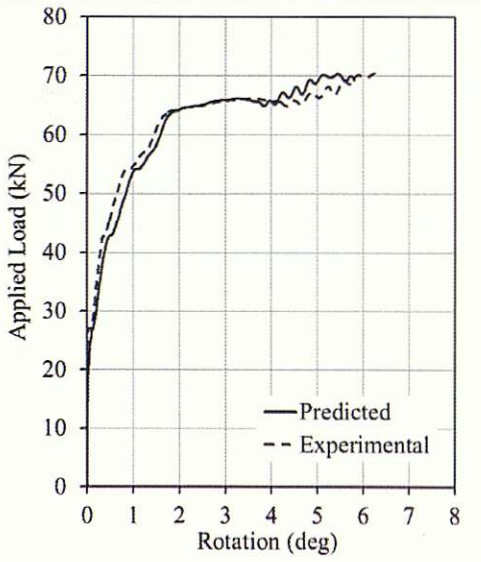

(f) Moment-rotation

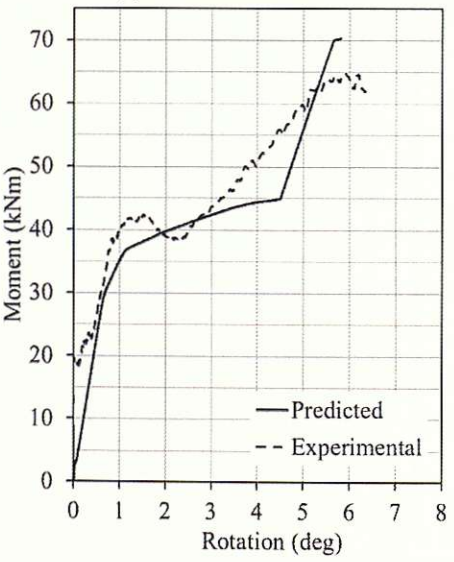

A1.3.4 Flexible end-plate test 5 (FEP5)

8mm thick endplate

Static test with single loading ram

(a) Moment-rotation

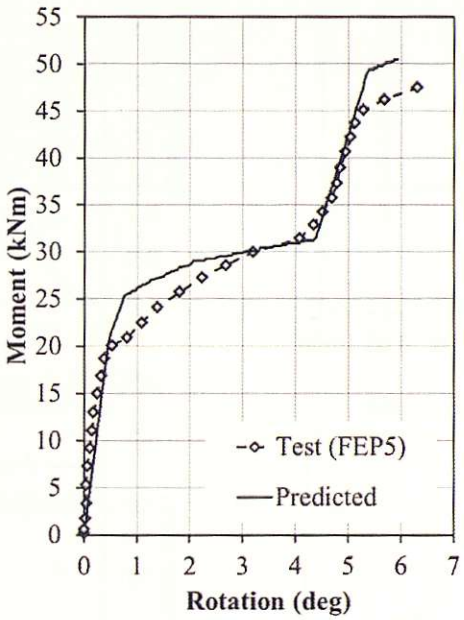

A1.3.5 Flexible end-plate test 6 (FEP6)

8mm thick endplate

Dynamic test with single loading ram

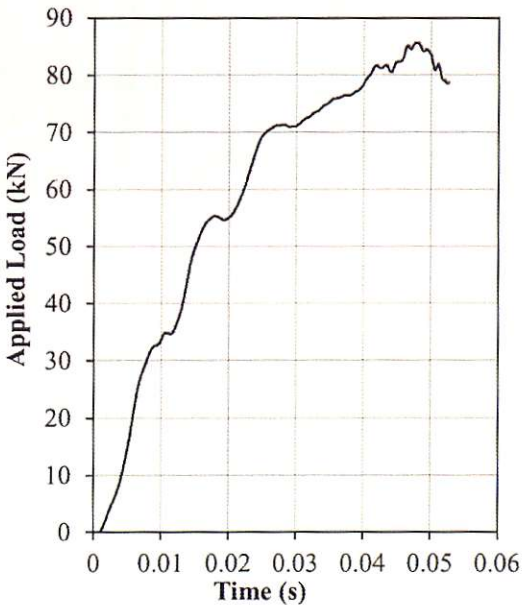

(a) Rotation-time

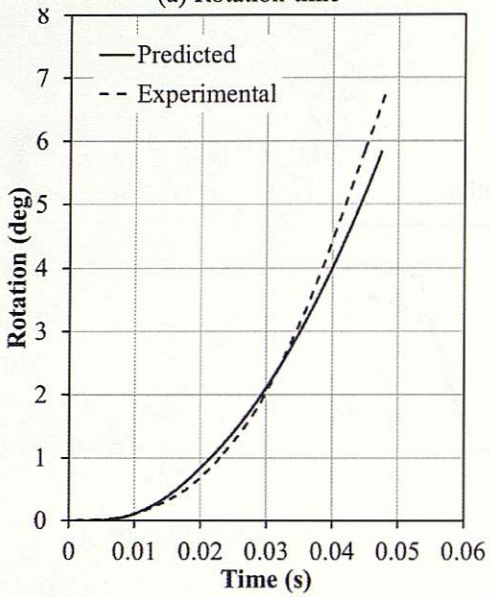

(b) Rotational velocity-time

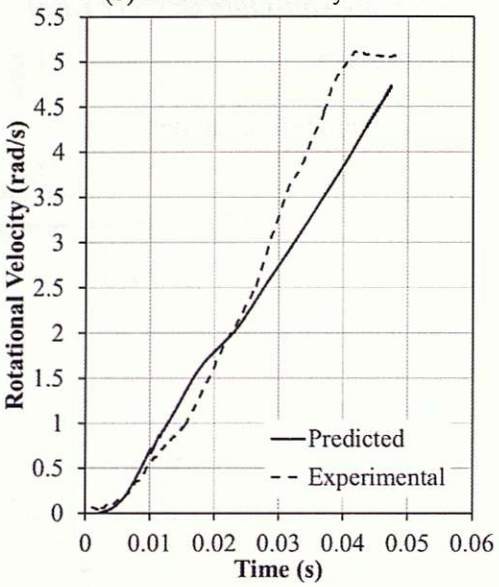

(c) Rotational acceleration-time

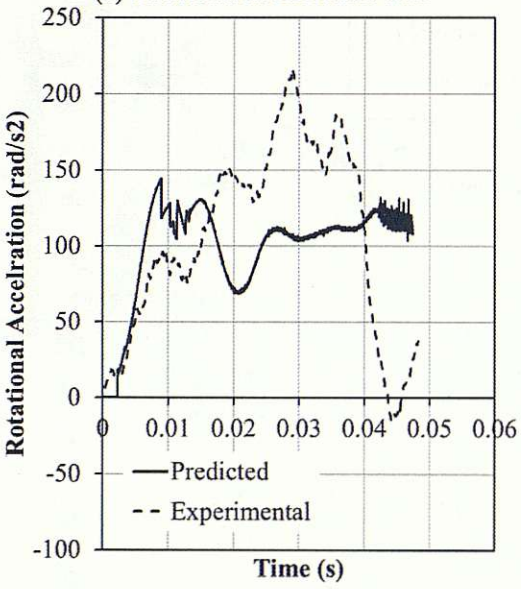

(d) Centre of mass displacement

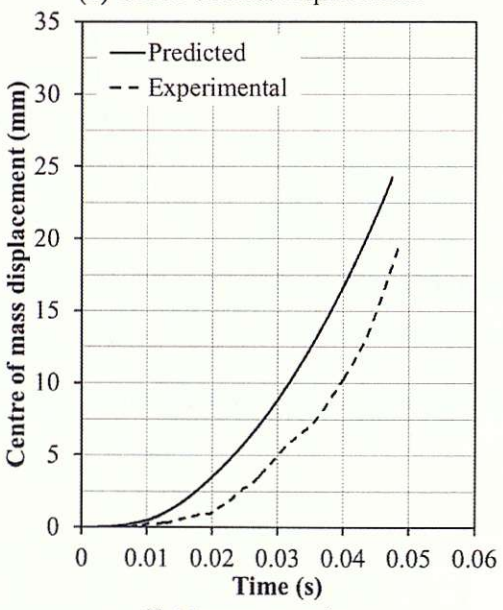

(e) Load-rotation

(f) Moment-rotation

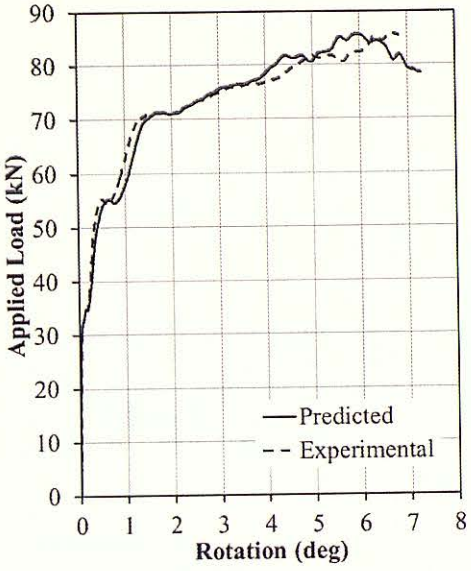

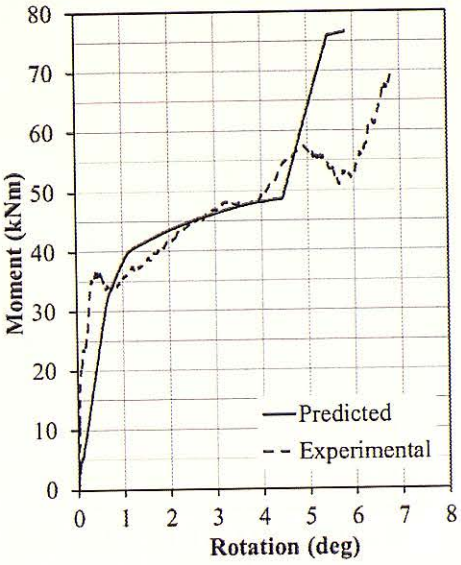

A1.3.6 Flexible end-plate test 9 (FEP9)

8mm thick endplate

Dynamic test with single loading ram

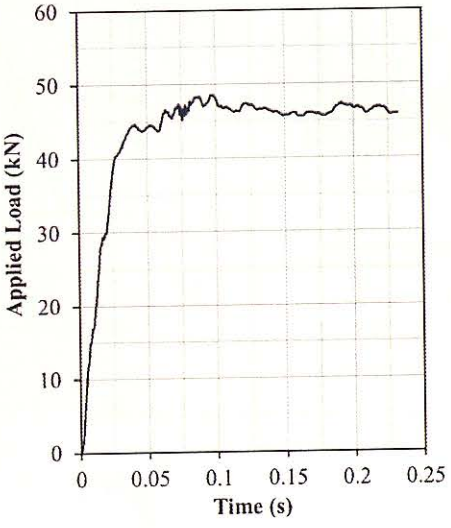

(a) Rotation-time

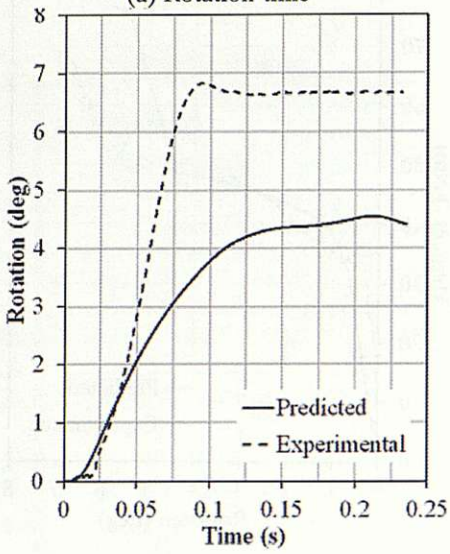

(b) Rotational velocity-time

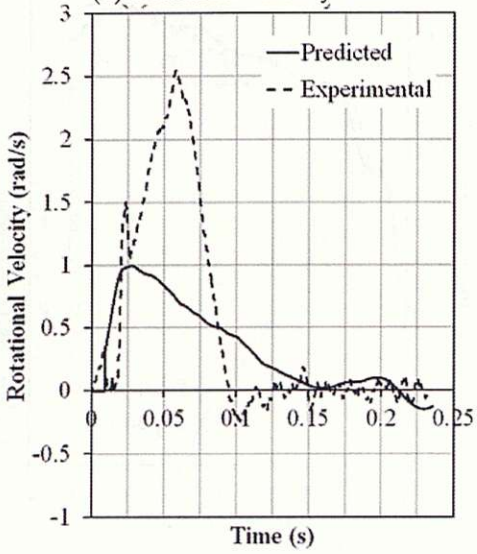

(c) Rotational acceleration-time

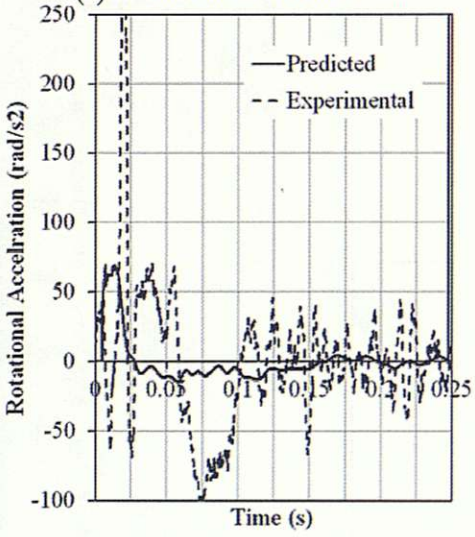

(d) Centre of mass displacement

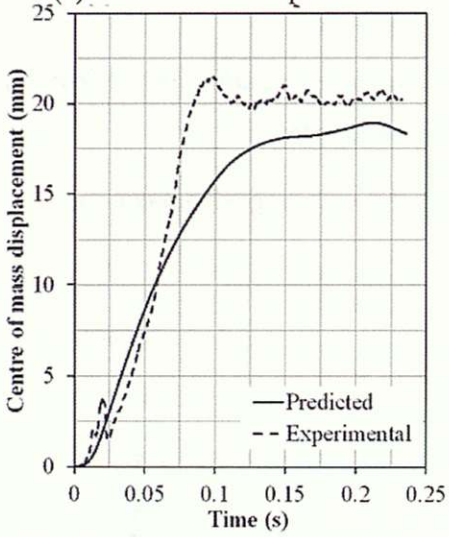

(e) Load-rotation

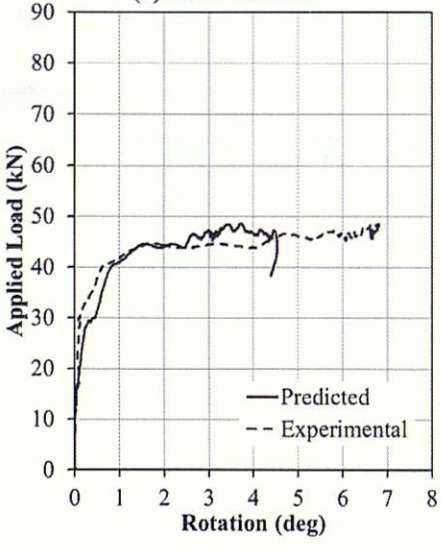

(f) Moment-rotation

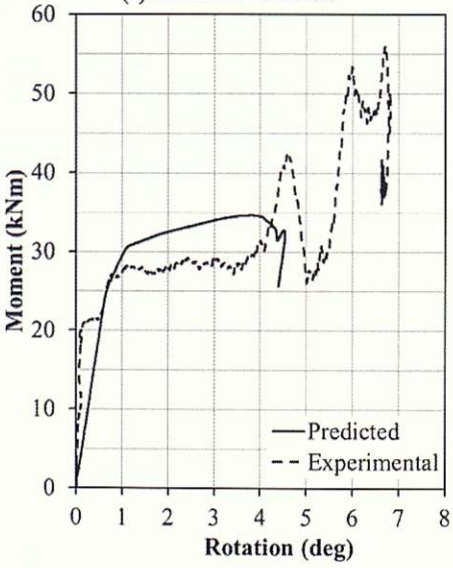

- Component-based method overestimates yield load at this loading rate
- This results in a stiffer connection and reduced rotation compared to the test result
- Both the test and prediction model show that the connection does not fail

A1.3.7 Flexible end-plate test 11 (FEP11)

10mm thick endplate

Dynamic test with single loading ram

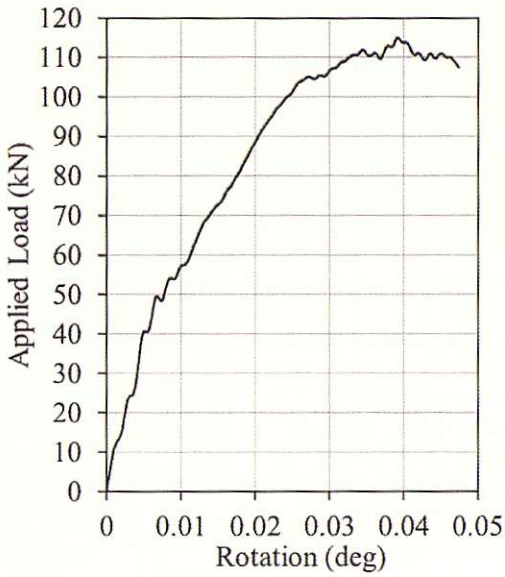

(a) Rotation-time

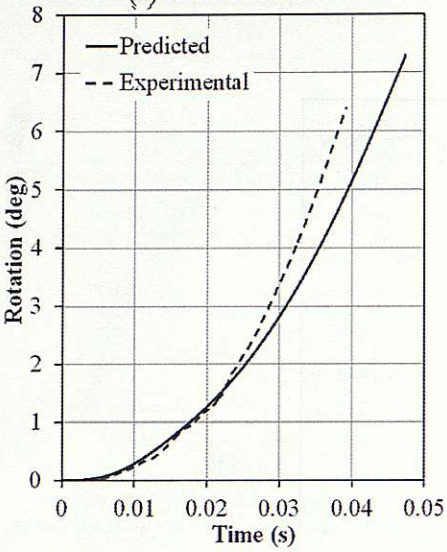

(b) Rotational velocity-time

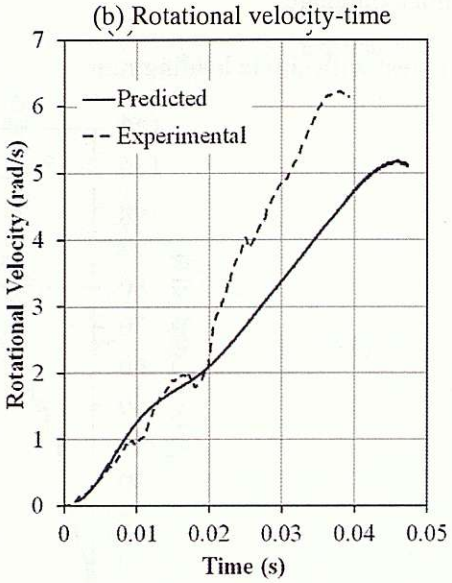

(c) Rotational acceleration-time

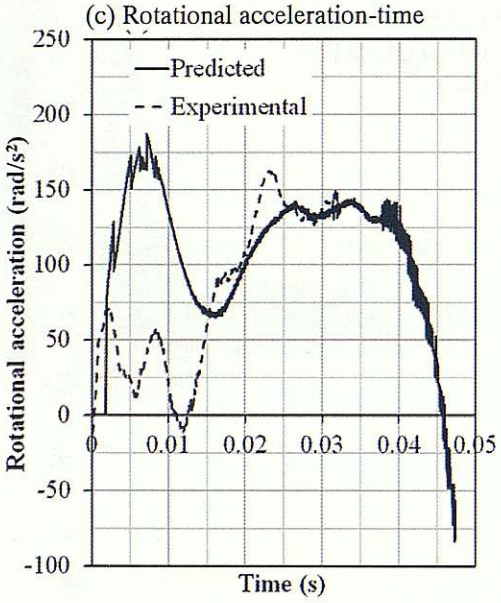

(d) Centre of mass displacement

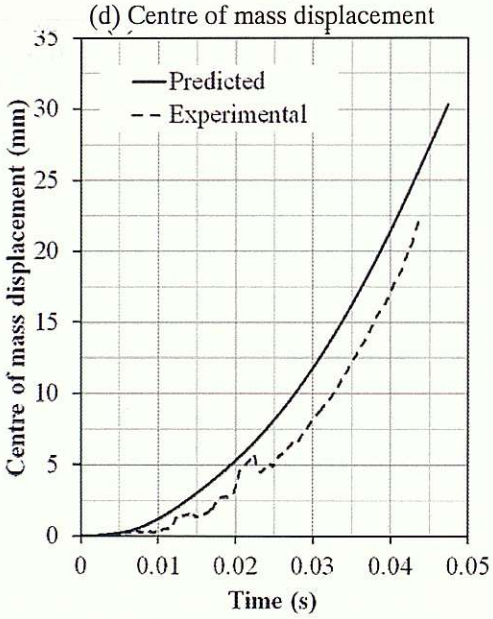

(e) Load-rotation

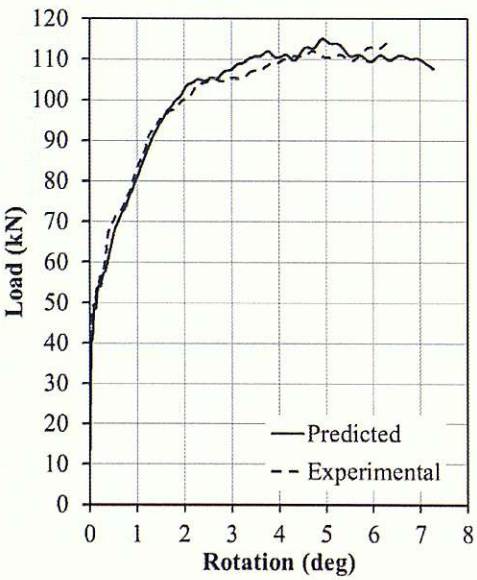

(f) Moment-rotation

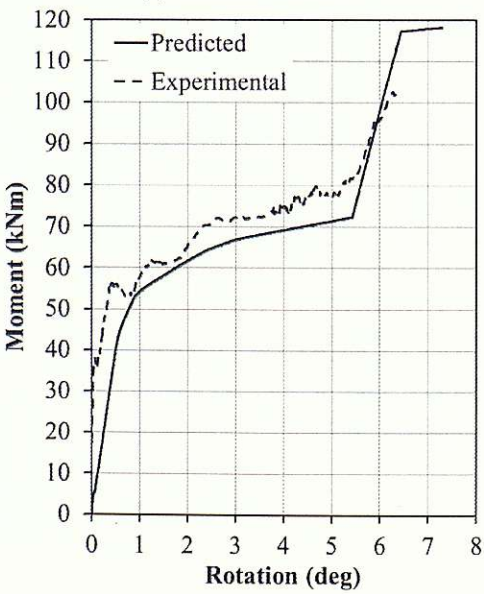

A1.3.8 Flexible end-plate test 14 (FEP14)

8mm thick endplate

Dynamic test with single loading ram

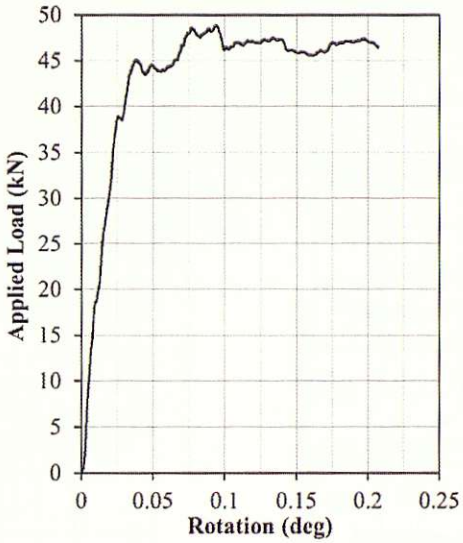

(a) Rotation-time

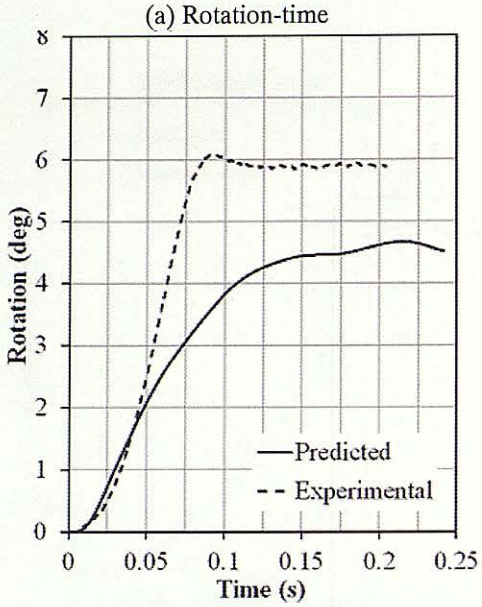

(b) Rotational velocity-time

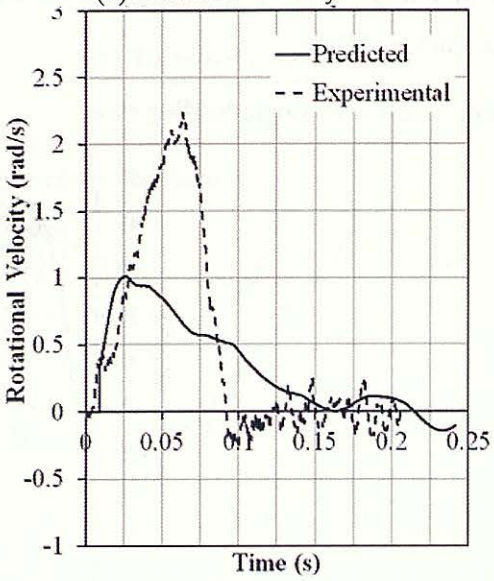

(c) Rotational acceleration-time

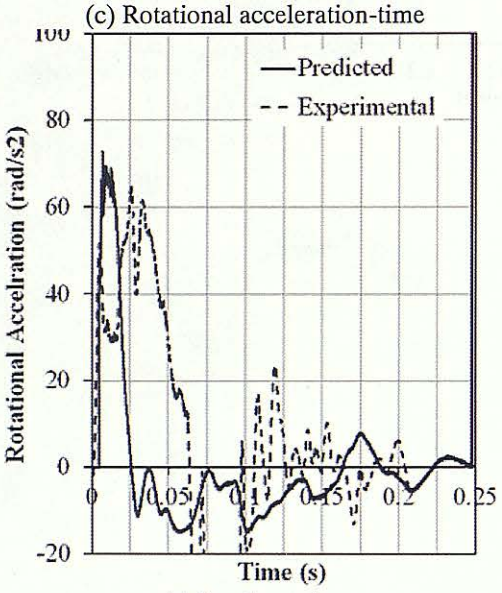

(d) Centre of mass displacement

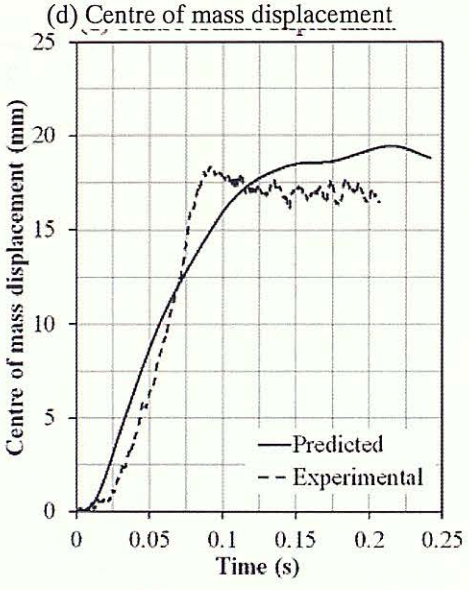

(e) Load-rotation

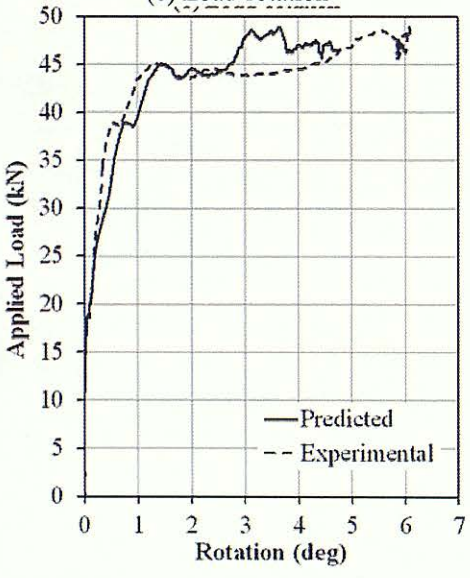

(f) Moment-rotation

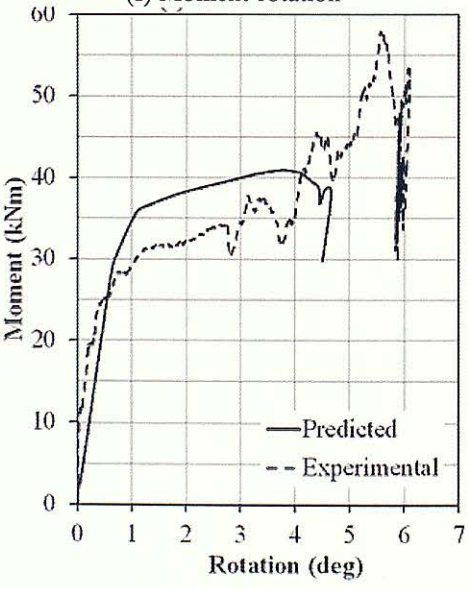

- No failure recorded in the test or prediction model
- Prediction model overestimates yield load at this loading rate resulting in stiffer connection and reduced rotation

A1.3.9 Flexible end-plate test 19 (FEP19)

8mm thick endplate

Dynamic test with dual loading rams for direct tension tests

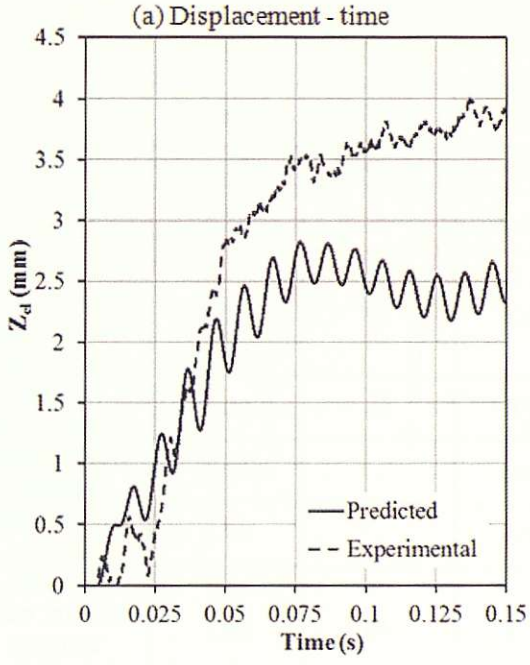

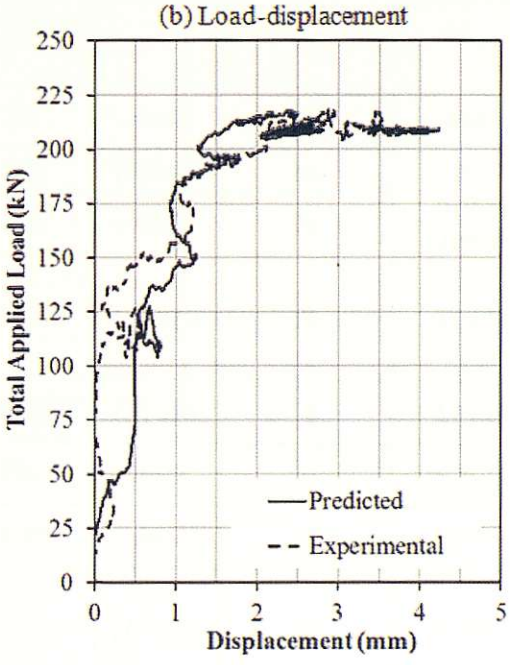

- No failure recorded in the test or prediction model
- Reasonable prediction of overall load-displacement behaviour but difficult to draw any definitive conclusions
- The predicted displacement-time history shows secondary oscillations of approximately 120Hz

A1.4 10mm FLEXIBLE ENDPLATE CONNECTIONS

Test Number	Endplate Thickness (mm)	Loading Type	Peak Moment (kNm)	Failure Rotation (deg)	Peak Loading Time (ms)	Peak applied axial load (kN)	Failure
FEP7	10	Dyn (B)	86.77	6.2	45	69.2	No Failure
FEP7 (cont)	10	Static	82.2	9.6	-	92.8	Fracture of endplate, beam web crushing and weld-endplate interface
FEP8	10	Static	98	13.2	-	116.7	Endplate fracture
FEP10	10	Dyn (B)	79.8	7.9	40	71.4	No
FEP10 (cont)	10	Static	76.6	11.5	-	89.5	Endplate fracture, bolt
FEP11	10	Dyn (E)	113.5	6.2	39	113.0	Endplate fracture, bolt, weld-endplate interface
FEP12	10	Dyn (C)	100.4	9.8	40	90.7	Endplate fracture, bolt
FEP13	10	Static	74.7	10.1	-	89.1	Weld-endplate interface
FEP15	10	Static	81.5	9.6	-	97.4	Weld-endplate interface
FEP17	10	Dyn (A)	91.4	7.1	40	87.1	Endplate fracture, weld-endplate interface

A1.4.1 Flexible endplate test 7 (FEP7)

10mm thick endplate

Dynamic test with single loading ram

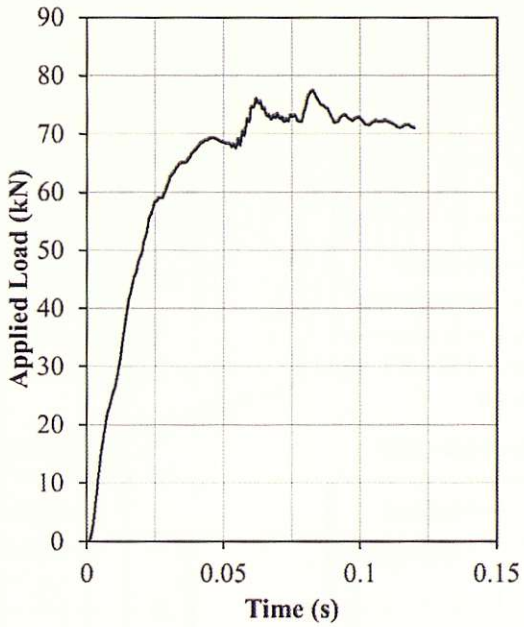

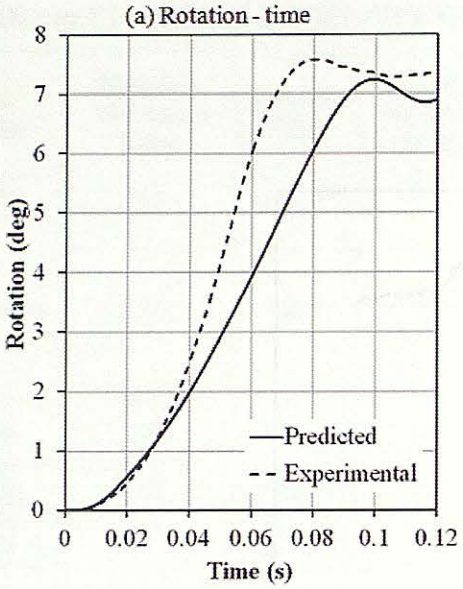

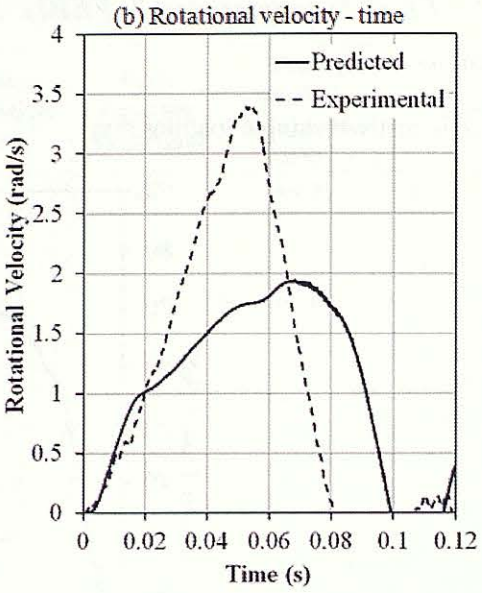

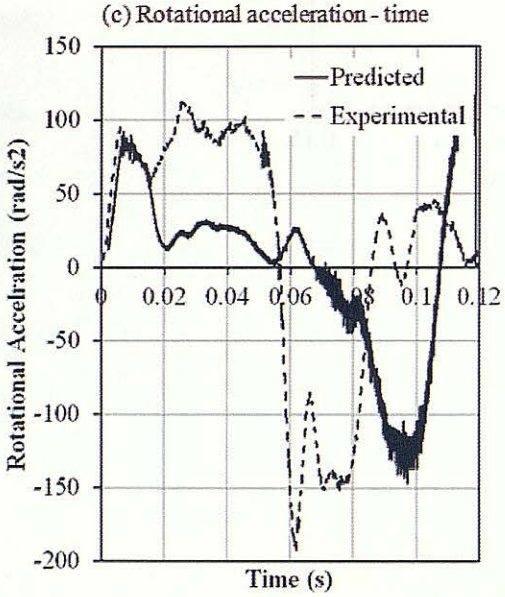

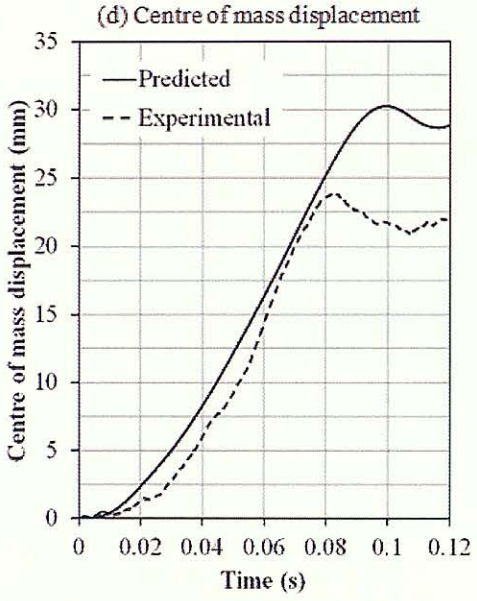

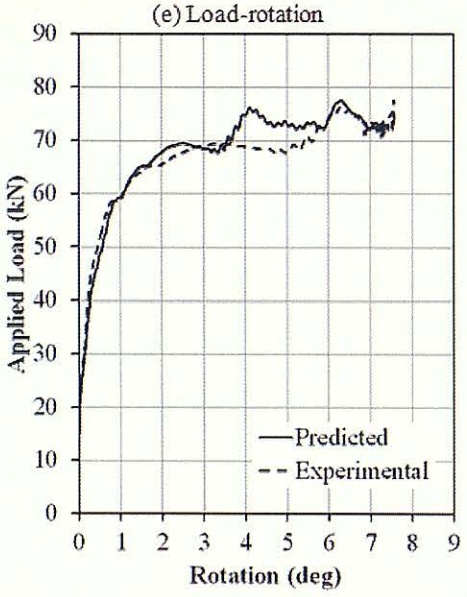

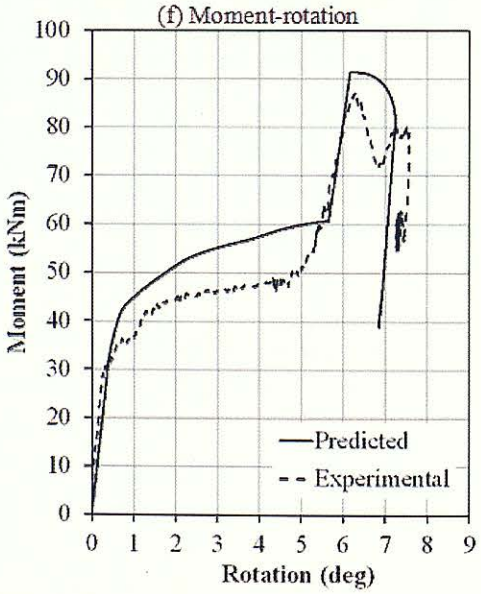

- No failure achieved in test

- Over prediction of yield moment and post yield stiffness

A1.4.2 Flexible endplate test 8 (FEP8)

10mm endplate

Static test with single loading ram.

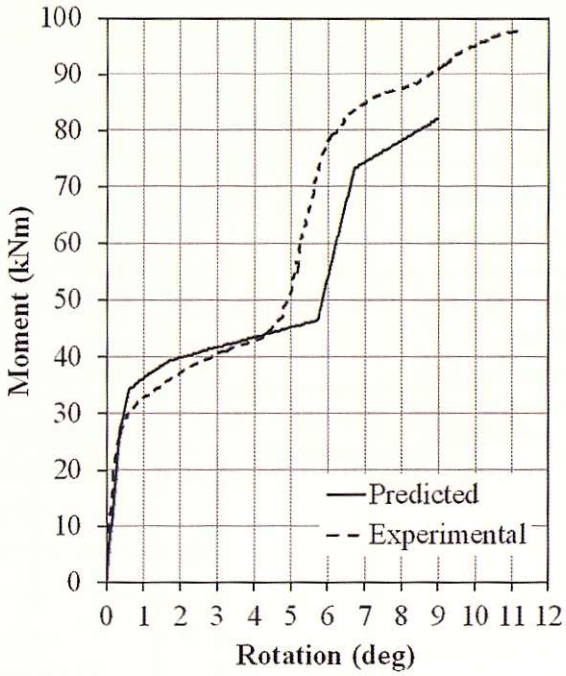

A1.4.3 Flexible endplate test 10 (FEP10)

10mm endplate

Dynamic test with single loading ram

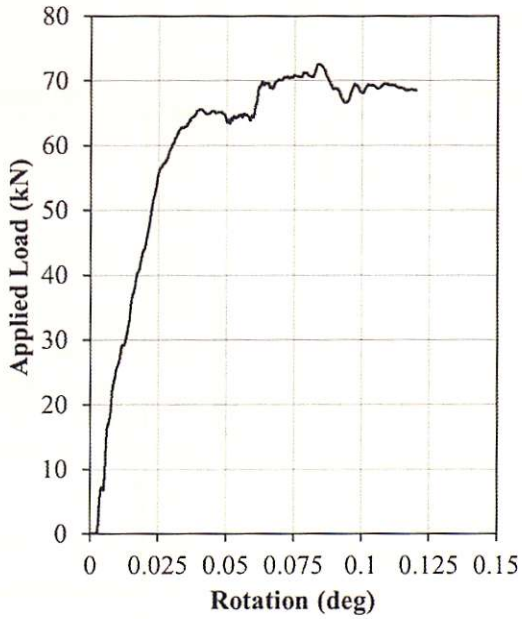

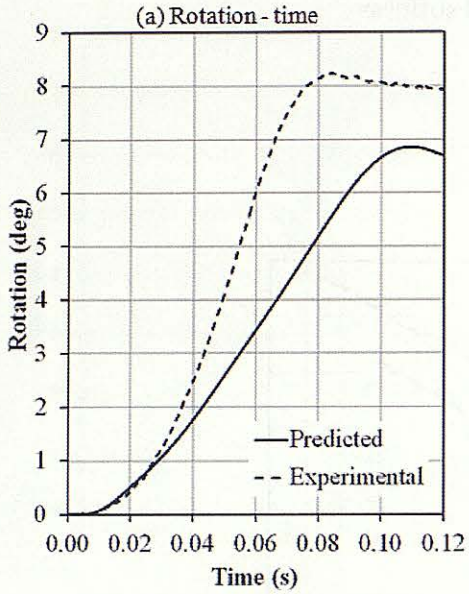

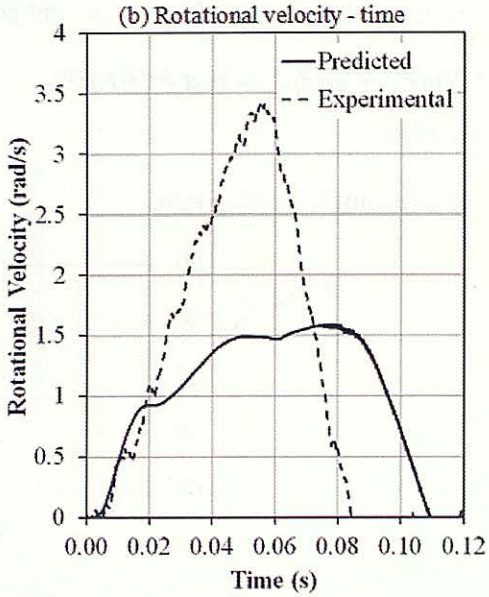

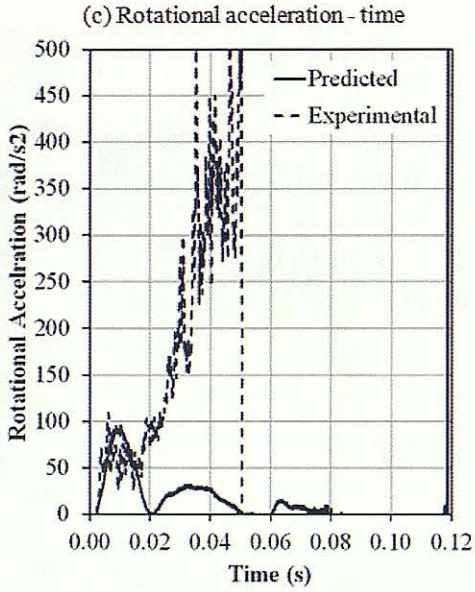

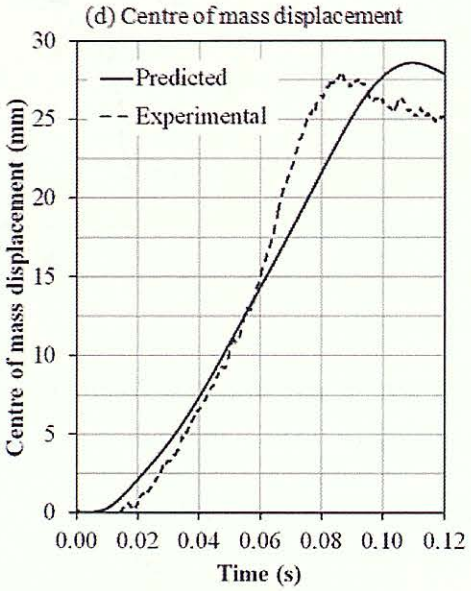

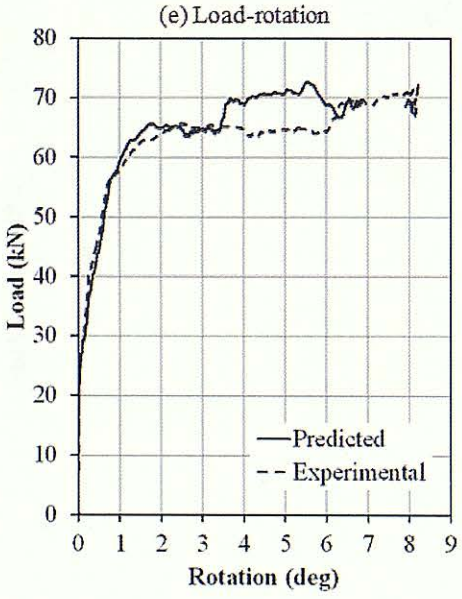

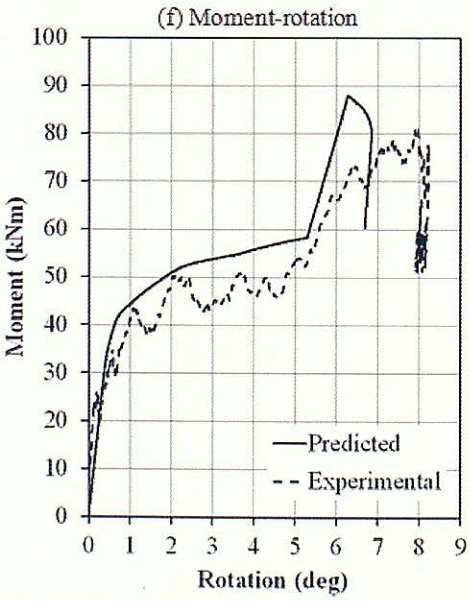

- No failure in experiment or prediction

A1.4.4 Flexible endplate test 11 (FEP11)

10mm thick endplate

Dynamic test with single loading ram

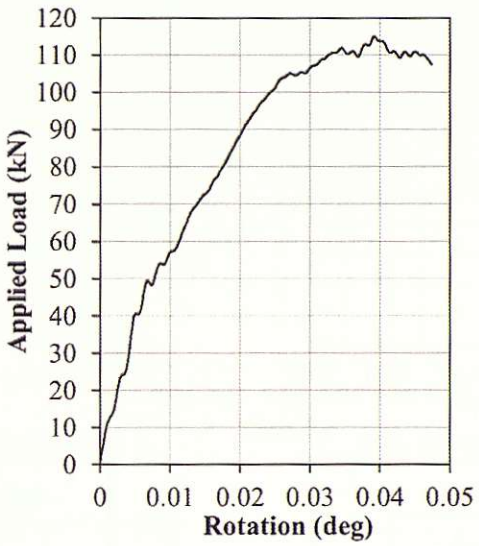

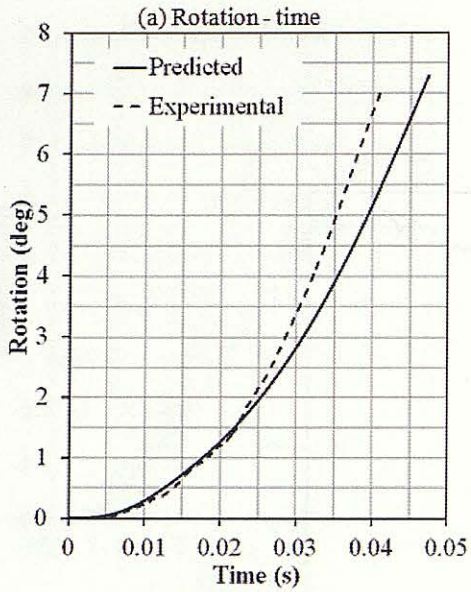
(a) Rotation - time
Predicted
Experimental
Rotation (deg)
Time (s)
0
1
2
3
4
5
6
7
8
0
0.01
0.02
0.03
0.04
0.05

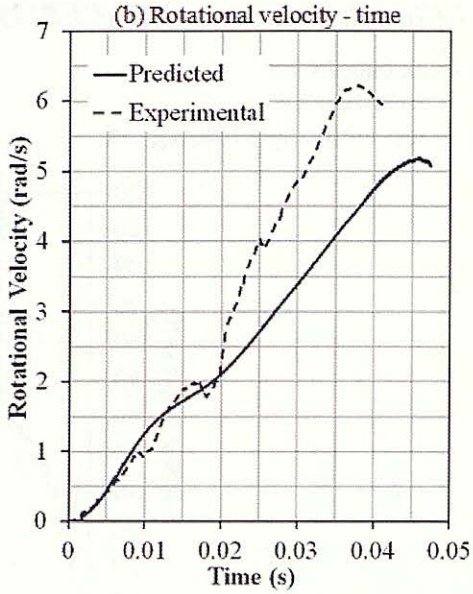
(b) Rotational velocity - time
Predicted
Experimental
Rotational Velocity (rad/s)
Time (s)
0
1
2
3
4
5
6
7
0
0.01
0.02
0.03
0.04
0.05

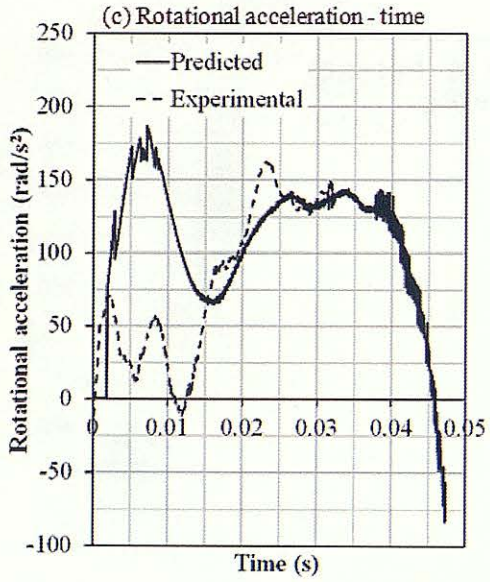
(c) Rotational acceleration - time
Predicted
Experimental
Rotational acceleration (rad/s²)
Time (s)
250
200
150
100
50
0
-50
-100
0
0.01
0.02
0.03
0.04
0.05

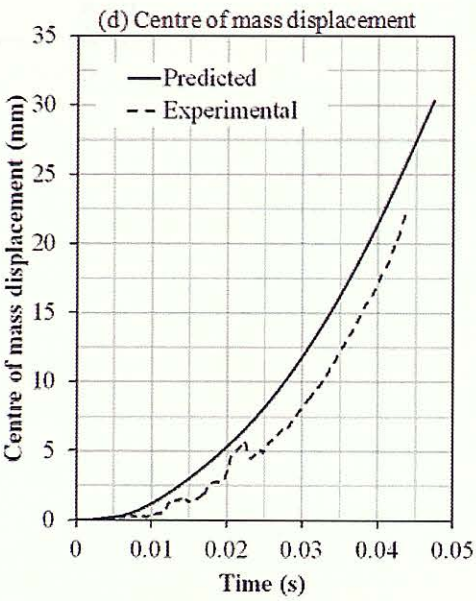
(d) Centre of mass displacement
Predicted
Experimental
Centre of mass displacement (mm)
Time (s)
35
30
25
20
15
10
5
0
0
0.01
0.02
0.03
0.04
0.05

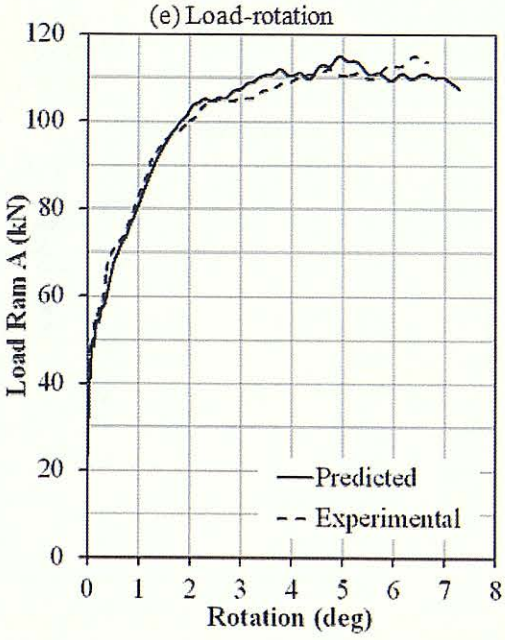
(e) Load-rotation
Predicted
Experimental
Load Ram A (kN)
Rotation (deg)
120
100
80
60
40
20
0
0
1
2
3
4
5
6
7
8

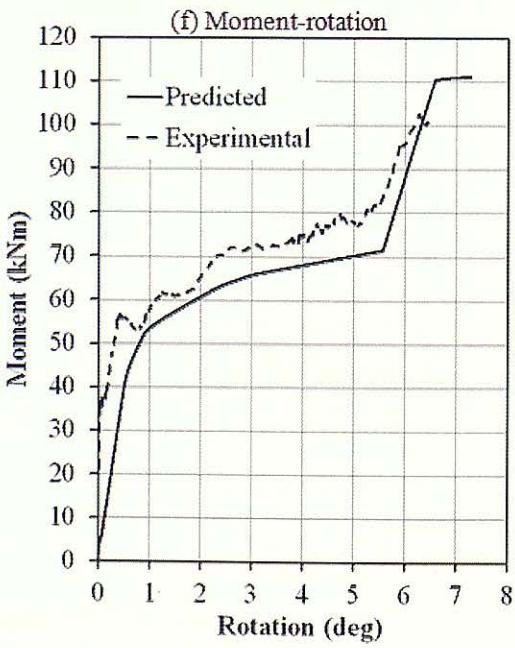
(f) Moment-rotation
Predicted
Experimental
Moment (kNm)
Rotation (deg)
120
110
100
90
80
70
60
50
40
30
20
10
0
0
1
2
3
4
5
6
7
8

A1.4.5 Flexible endplate test 12 (FEP12)

Dynamic test with single loading ram

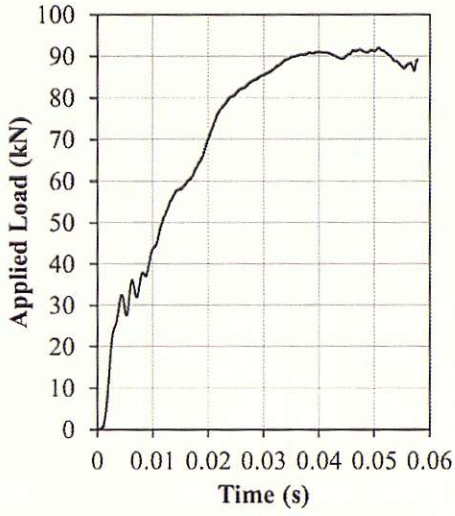

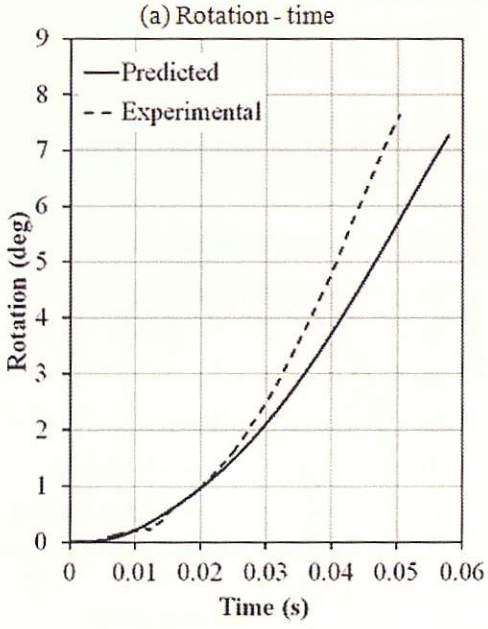

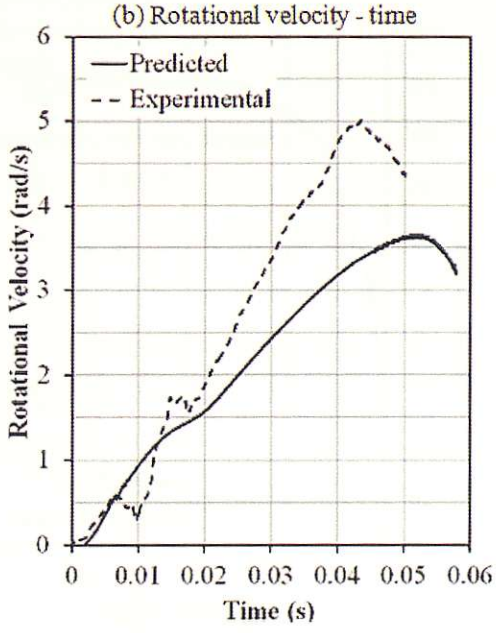

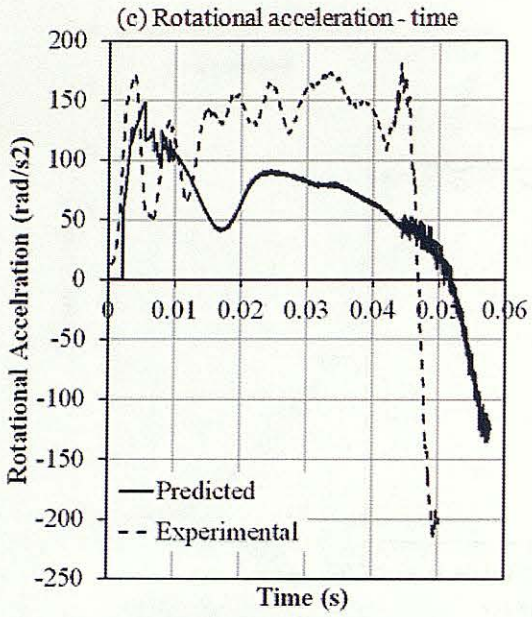
(c) Rotational acceleration - time
Rotational Acceleration (rad/s2)
Time (s)
Predicted
Experimental

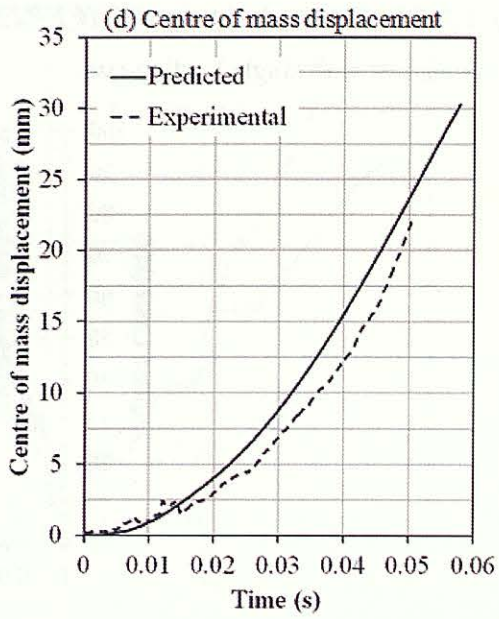
(d) Centre of mass displacement
Centre of mass displacement (mm)
Time (s)
Predicted
Experimental

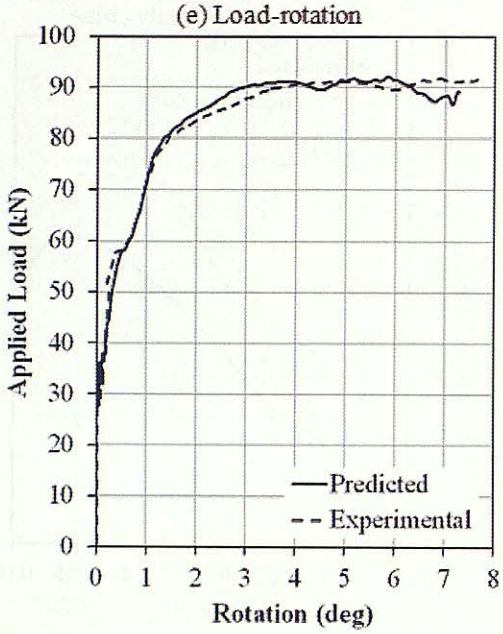
(e) Load-rotation
Applied Load (kN)
Rotation (deg)
Predicted
Experimental

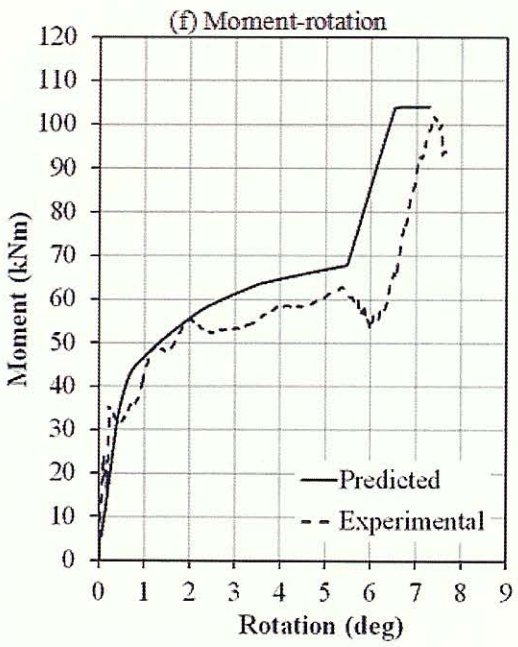
(f) Moment-rotation
Moment (kNm)
Rotation (deg)
Predicted
Experimental

A1.4.6 Flexible endplate test 15 (FEP15)

Static single ram test

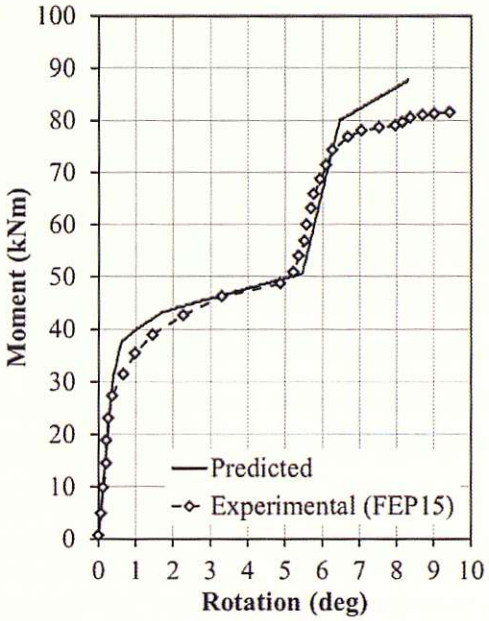

- Close prediction of yield moment, plastic stiffness and ultimate capacity
- Bearing rotation is over predicted by approximately ½ degree

A1.4.7 Flexible endplate test 17 (FEP17)

Dynamic test with single load ram

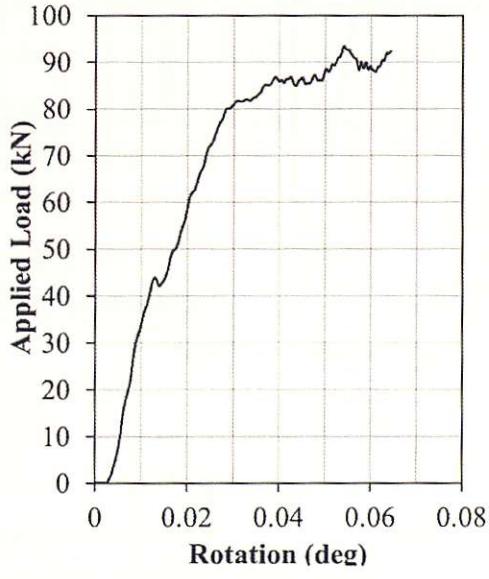

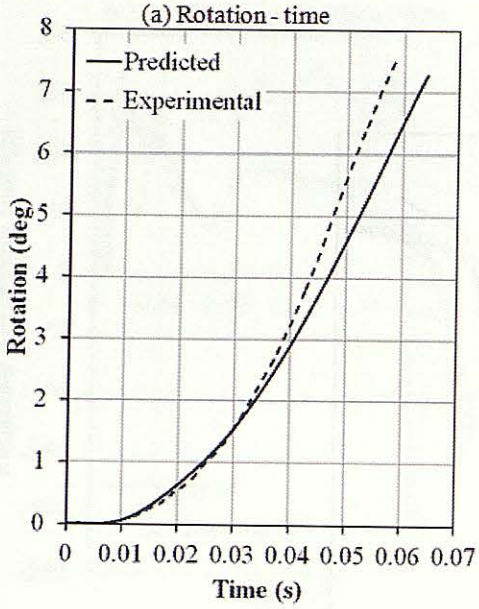
(a) Rotation - time
Predicted
Experimental
Rotation (deg)
Time (s)
0 1 2 3 4 5 6 7 8
0 0.01 0.02 0.03 0.04 0.05 0.06 0.07

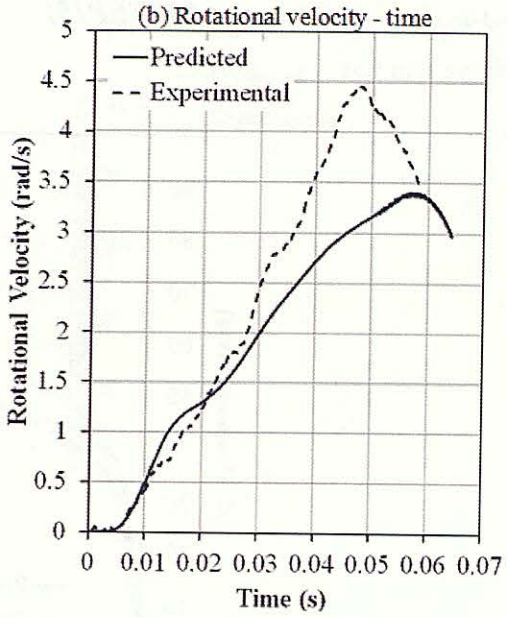
(b) Rotational velocity - time
Predicted
Experimental
Rotational Velocity (rad/s)
Time (s)
0 0.5 1 1.5 2 2.5 3 3.5 4 4.5 5
0 0.01 0.02 0.03 0.04 0.05 0.06 0.07

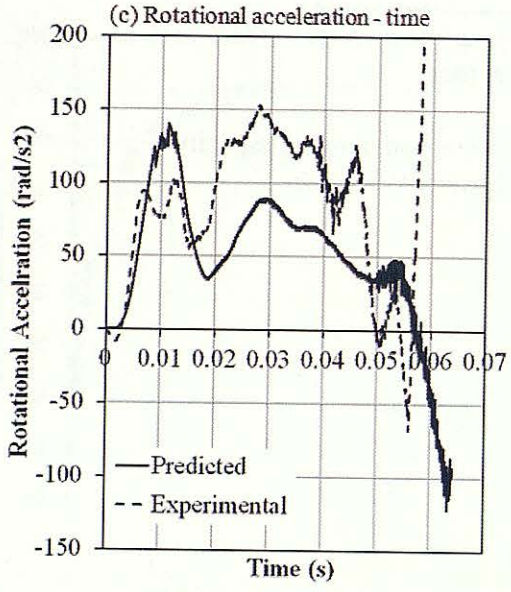
(c) Rotational acceleration - time
Predicted
Experimental
Rotational Acceleration (rad/s2)
Time (s)
200 150 100 50 0 -50 -100 -150
0 0.01 0.02 0.03 0.04 0.05 0.06 0.07

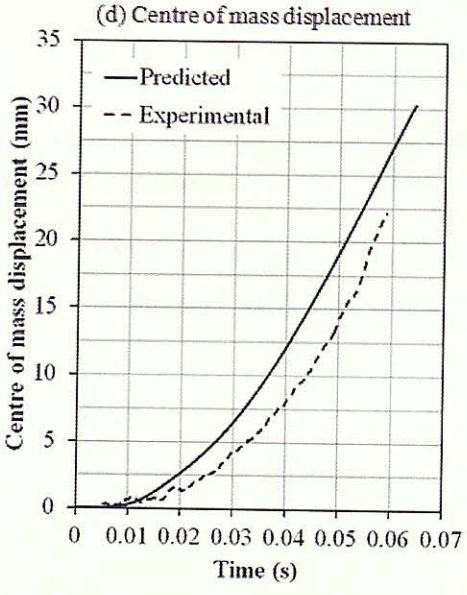
(d) Centre of mass displacement
Predicted
Experimental
Centre of mass displacement (mm)
Time (s)
0 5 10 15 20 25 30 35
0 0.01 0.02 0.03 0.04 0.05 0.06 0.07

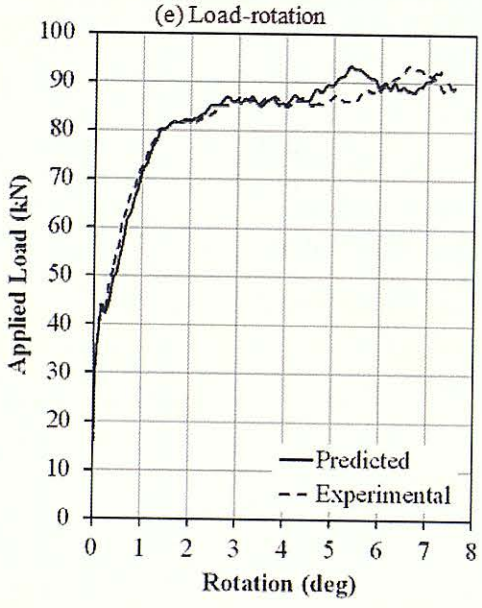
(e) Load-rotation
Predicted
Experimental
Applied Load (kN)
Rotation (deg)
0 10 20 30 40 50 60 70 80 90 100
0 1 2 3 4 5 6 7 8

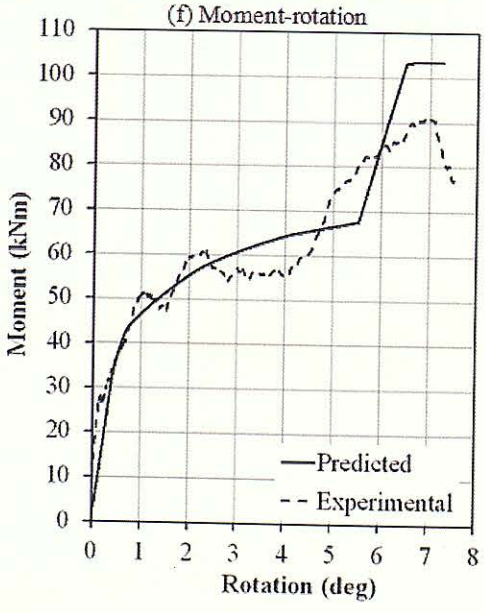
(f) Moment-rotation
Predicted
Experimental
Moment (kNm)
Rotation (deg)
0 10 20 30 40 50 60 70 80 90 100 110
0 1 2 3 4 5 6 7 8

B1. Single Degree of Freedom (SDOF) Methods

B1.1 Introduction

An investigation into current methods of structural analysis relating to the field of blast and explosion loading is presented. In addition a review of blast phenomena is conducted to provide background to the threat and expected loading conditions.

A common method for analysis of blast effects on structures is the single degree of freedom method (SDOF); which simplifies the behaviour of a structure or structural element to one point in the element with an equivalent mass and stiffness. The single displacement variable of this model can be found and then used to assess the behaviour of the system. SDOF systems have been widely used to predict the effect of blast on a structure. TM5-1300 (1990) - *Structures to resist the effects of accidental explosions*, presents methods of design for structures to resist blast loading based on SDOF systems. The method is based upon early work by Biggs (1964). Mays and Smith (1995) provide an explanation of the basis of equivalent SDOF systems and the application of these techniques to the design of elements is demonstrated for steel and concrete.

The equivalent single degree of freedom method uses the conservation of energy, internal strain energy and virtual work to create an equivalent lumped mass-spring system. The transformation factors used to determine the equivalent mass, resistance and loading are based upon the deflected shape function of the system and the distribution of mass and loading over the original structure. The dynamic reactions of the element can be calculated using dynamic equilibrium.

An example of an equivalent SDOF system is shown in Figure 1-1.

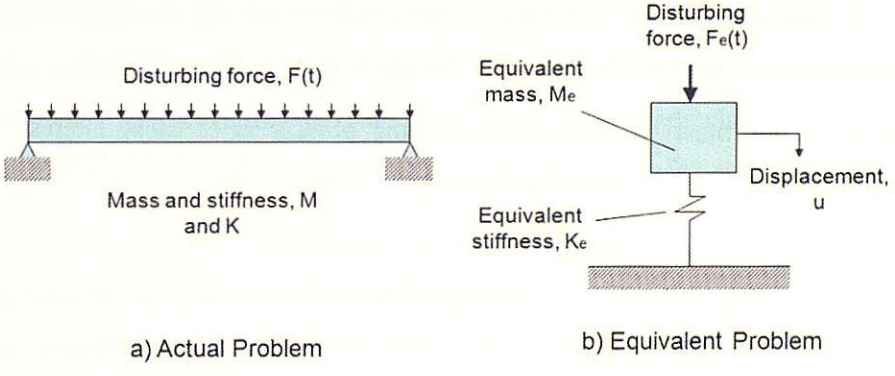

Figure 1-1: SDOF system

The equation of motion for the equivalent system is shown in Equation B1. Note that it is general practice to ignore damping due to the short load duration.

$$M_E\ddot{u} + k_E u = F_E(t) \qquad \text{B1.}$$

Where M_E, k_E, u and $F_E(t)$ have the same meanings shown in Figure 1-1. Further analysis of the method is presented in Section B1.3 but first expected loads need to be characterised.

B1.2 Background to the threat

B1.2.1 Mechanism of a blast or explosion

In order to design structures to resist blast loading, the blast itself must be quantified. An explosion is essentially an extremely rapid release of stored potential energy. How this energy is stored defines the classification of the explosive. For example the rupture of a pressure vessel can result in shock waves within the air in what is often referred to as a mechanical explosion. Of interest in this thesis is the use of chemical explosives; where the energy is stored within the explosive material as chemical bonds. In general there are two main types of chemical explosive; high and low.

A high explosive material can be defined by a shock wave travelling through the explosive material faster than the speed of sound which is known as detonation [Tyas (2010)]. Once the initial chemical bonds are broken and energy is released, the pressure rises in the explosive instantaneously. This increase in pressure causes surrounding bonds to be broken thus starting a chain reaction until the resistance of the unreacted explosive balances the driving force of the reacting material. These steady state conditions define the detonation wave speed for the explosive. This speed is often used to indicate the power of the explosive.

The release of energy in a hydrocarbon explosion is significantly slower than that of a high explosive. Typically the oxygen required is not stored within the chemical compound and thus the chemical reaction is usually driven by the rapid burning of fuel with oxygen from the surrounding air. This process is called deflagration and the intensity of the explosion is dictated by the fuel-air mixture. The ideal percentage mixture for each fuel is called the stoichiometric mixture.

In either case once the reaction reaches the charge or fuel edge there is no more reactant to perpetuate the reaction and the wave enters the surrounding air. The resulting wave of pressure within the air is called the air blast. For a high explosive this wave can typically propagate at a rate of 8000 m/s whilst for a hydrocarbon explosive this figure is more often 2000 m/s.

The interaction of this blast wave with surrounding objects is of most interest to structural engineers as this is what constitutes the blast loading.

B1.2.2 Determining the design characteristics of a blast load

Two key aspects of a blast wave are the incident or side-on pressure and the reflected pressure. The incident pressure (P_i) is that associated with a blast wave travelling unimpeded in free air or parallel to a surface. The reflected pressure (P_r) is that which develops upon contact with a rigid target. This includes the effect of the air particles in the blast wave being brought to rest and conversion of their kinetic energy to an increase in air density. Thus the reflected pressure is always higher than the incident pressure. The term overpressure is used to define the pressure over and above normal atmospheric pressure (P_a).

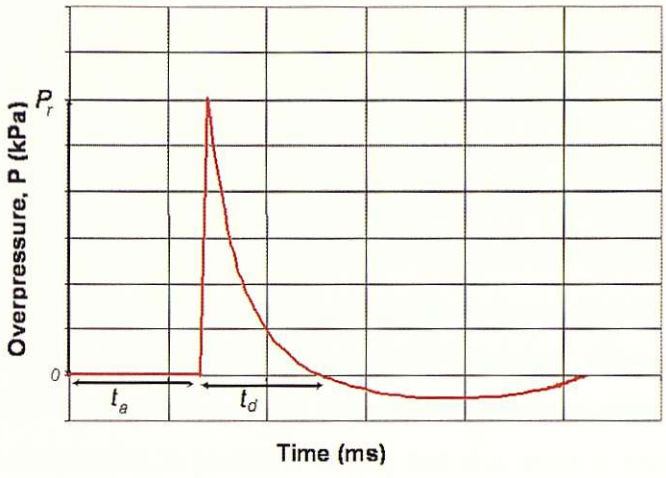

Figure 1-2: Typical pressure-time history

The time of arrival (t_a) is the time that the blast wave strikes the rigid surface and the length of time this pressure acts is called the time of duration (t_d). As can be seen from Figure 1-2 the pressure then becomes negative and reverse loads the object. Although this can be important for long duration loads (i.e. hydrocarbon or gas explosions) it is often disregarded for high explosives where the principal damage is assumed to be caused by the very high peak pressures. A final important parameter of a blast wave is the specific impulse (i_r) which can be found by integrating the pressure over the loading duration. The actual total impulse can then be calculated by multiplying this by the area of the impacted target.

The methods of predicting these parameters fall into three categories:

- Mathematical
- Empirical
- Numerical

The mathematical methods provide a closed form solution of the shock equations in air [Tyas (2010)]. Once formulated these are quick to perform but have limited applicability. Air is assumed to behave as an ideal gas travelling with a shock speed U perpendicular towards a target. This assumption works well for far-field explosions but breaks down for very high intensity shock waves.

Mach number

$$M = \frac{U}{a}$$

Where a is the ambient wave speed in air

U is the shock front velocity

B2.

Incident pressure

$$P_i = \left[\frac{7(M^2 - 1)}{6}\right] P_a$$

B3.

Reflected pressure

$$P_r = \frac{8M^2 + 4}{M^2 + 5} P_i \qquad \text{B4.}$$

Unfortunately even simple situations such as a real spherical shock cannot be calculated using this method so alternatives have been developed.

Following World War II the USArmy (1946) produced a report entitled "*Effects of impact and explosion*" which analysed the work conducted on high explosives during the war and details the estimation of pressures and impulses. This method is an empirical approach first noted by Hopkinson in 1915 which uses what is referred to as cube-root scaling which Baker, Cox et al. (1983) describe as:

> "*Self-similar blast waves are produced at identical scaled distances when two explosive charges of similar geometry and of the same explosive but of different sizes are detonated in the same atmosphere*".

This allows the use of a scale distance parameter z to predict peak pressures as long as the equivalent weight of charge in TNT is known. This system works because as the spherical blast wave expands in three dimensions, the energy density associated with the wave decreases by the same factor. The energy of the explosion is directly proportional to the charge mass therefore a scaled distance can be used.

Scaled distance

$$z = \frac{s}{\sqrt[3]{W}} \qquad \text{B5.}$$

s = standoff distance (m)
W = charge mass (kg)

A convenient way of presenting blast wave parameters is to use charts produced from experimental data plotted against scaled distance. Suitable charts can be found in TM5-1300 (1990) and Mays and Smith (1995) and programs such as CONWEP use these to produce solutions for problems with simple geometry. These provided a quick way of gaining initial estimates of the blast pressures, however a big drawback is the inability to include the interaction effects of other structures or more complex geometry.

The solution is either experimental work or to numerically model the air blast. Air3d is a piece of software developed at Cranfield University as part of the project "*An approach to the evaluation of blast loads on finite and semi-infinite structures*" by Rose (2001). The program uses a variant of the Advection Upstream Splitting Method as devised by Wada (1997) to solve the Euler equations in three-dimensions. The software can be used to investigate the interaction of objects and shapes within a blast area and provides pressure-time history over the period of the blast.

Once the peak pressure on a structural element is calculated it is converted to an equivalent force by multiplying by the area over which it acts and thus a force-time relationship can be predicted.

B1.3 The equivalent method and its uses

The Equivalent SDOF method will be reviewed and used to evaluate a structural system. The US Army Corps of Engineers, USACE (1957), outlines the foundation for this method as well as providing a detailed explanation for the use of a shape function for the deflected shape. This is used to predict the deflection at all points on the original structure from the single displacement in the lumped mass-spring system. Theoretically if the shape function used to calculate the transformation factors is correct then the response of the SDOF system will replicate the resulting displacement for that reference point in the structure exactly. However as the shape function is found from the deflected shape it is not possible to predict it exactly and thus assumptions have to be made. The accuracy of the approach is thus dependent on the chosen deflected shape. The most common approximation is to use the static deflected shape under the same uniformly distributed load from the blast loading, however other functions can be used. The use of transformation factors can then be used to simplify Equation B6:

$$K_M M\ddot{u} + K_s ku = K_L F(t) \qquad \text{B6.}$$

Where:

K_M = mass transformation factor

M = mass of structure

K_L = load transformation factor

K_S = stiffness transformation factor

k = stiffness

k_e = equivalent stiffness

F = loading

The calculation of these transformation factors is done by equating the work done (WD), internal strain energy (U) and kinetic energy (KE) of the two systems. The equivalent system will have the same maximum displacement (u_{max}) and initial velocity ($\dot{u}$) as the actual problem. Reducing the displacements of a multi degree of freedom system to a single displacement variable requires the assumption of a deflected shape. As an example the fundamental mode of a simply supported beam will be used to demonstrate kinematic equivalence between the distributed and equivalent systems. The deformed shape for the fundamental mode is:

$$u(x) = u_{max} \sin\left(\frac{\pi x}{L}\right) \qquad \text{B7.}$$

Evaluating *WD and KE* for this deformed shape gives:

$$WD = \int_0^L F(t)u(x)^2\,dx = \frac{2}{\pi}F(t)u_{max}L \qquad \text{B8.}$$

$$KE = \frac{\rho A}{2}\int_0^L u(x)^2\,dx = 0.25\,\rho AL\,{u_{max}}^2 \qquad \text{B9.}$$

$$U = \frac{1}{2}\int_0^L EI\frac{\delta u^2(x)^2}{\delta x^2}\,dx = \frac{\pi^4 EI\,{u_{max}}^2}{4\,L^3} \qquad \text{B10.}$$

The same energies are calculated for the equivalent system in Figure 1-1 (b) from simple spring theory giving:

$$WD = F_E(t)u_{max} \qquad \text{B11.}$$

$$KE = 0.5\,M_e{u_{max}}^2 \qquad \text{B12.}$$

$$U = 0.5k_e{u_{max}}^2 \qquad \text{B13.}$$

Equating the equations for the actual system to the equivalent ones and recognizing that $\rho AL = M$ (total mass of the beam) and FL is the total beam static load provides:

Load Factor from work done

$$K_L = \frac{F_E}{F} = \frac{WD\,2\,u_{max}}{WD\,\pi\,u_{max}} = \frac{2}{\pi} = 0.6366 \qquad \text{B14.}$$

Mass Factor from kinetic energy

$$K_M = \frac{M_E}{M} = \frac{2KE{u_{max}}^2}{4KE{u_{max}}^2} = 0.5 \qquad \text{B15.}$$

Equivalent stiffness from strain energy

$$k_e = \frac{\pi^4 EI\,{u_{max}}^2}{4\,L^3} \div 0.5{u_{max}}^2 = \frac{\pi^4 EI}{2\,L^3} \qquad \text{B16.}$$

Actual beam stiffness for simply supported beam from TM5-1300 (1990) table 3-8:

$$k = \frac{384EI}{5\,L^3} \qquad \text{B17.}$$

Stiffness Factor

$$K_S = \frac{k_e}{k} = \frac{\pi^4 EI}{2\,L^3} \div \frac{384EI}{5\,L^3} = \frac{5\pi^4}{2 * 384} = 0.634 \qquad \text{B18.}$$

These relationships have been developed based upon the maximum displacement and the kinematic equivalence of the two systems. The frequency of the equivalent system will now be compared

against the frequency for the fundamental mode of the actual problem. The exact solution is given by Baker, Cox et al. (1983) as:

$$\omega = \pi^2 \sqrt{\frac{EI}{ML^3}} \qquad \text{B19.}$$

For the equivalent system,

$$\omega = \sqrt{\frac{k_E}{M_E}} = \sqrt{\frac{\pi^4 EI}{2\ L^3 0.5M}} = \pi^2 \sqrt{\frac{EI}{ML^3}} \qquad \text{B20.}$$

This shows that assuming the fundamental mode for the deformed shape gives a natural frequency equal to the beam's fundamental frequency and that the equivalent system's behaviour is correct.

The same process as detailed above can be done for assuming the deformed shape of the statically deflected shape given below:

Static deflected shape

$$u = \frac{16u_{max}}{5L^4}(x^4 - 2Lx^3 + L^3x) \qquad \text{B21.}$$

Equating the energies of the two systems gives the following results.

$K_M = 0.50$

$K_L = 0.64$

$k_e = 0.64k$ therefore $K_S = 0.64$

The stiffness of the equivalent system is the internal force trying to restore it to its static position therefore it can be shown that the stiffness factor should always equal the load factor.

$$K_S \approx K_L \qquad \text{B22.}$$

Using these modified stiffness and mass factors, the frequency of the equivalent system is now:

$$\omega = 9.889 \sqrt{\frac{EI}{ML^3}} \qquad \text{B23.}$$

Some difference is to be expected between the static deformed shape and the fundamental mode frequency due to the inclusion of other modes other than the first however this value is still within 0.2 percent.

To reduce the number of coefficients required for analysis, it is common to define a load-mass factor, K_{LM}, where:

$$K_{LM} = \frac{K_M}{K_L} \qquad \text{B24.}$$

Using these new parameters, Eqn 3.6 can then be simplified as follows.

$$K_{LM} M\ddot{u} + ku = F(t) \qquad \text{B25.}$$

The equivalent system equation of motion can therefore be found using a single transformation factor and assumed deflected shape. Under the loading, the system may undergo a change of state from elastic through to plastic and a similar method can be done to produce transformation factors for both plastic and elastic deformations with a variety of support and loading conditions as shown in Figure 1-3. It should be noted that although a coefficient is applied to the mass to give an equivalent mass, the actual stiffness of the element is used throughout the analysis.

Edge Conditions and Loading Diagrams	Range of Behavior	Load Factor K_L	Mass Factor K_M	Load-Mass Factor K_{LM}
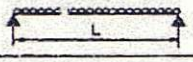	Elastic Plastic	0.64 0.50	0.50 0.33	0.78 0.66
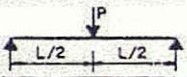	Elastic Plastic	1.0 1.0	0.49 0.33	0.49 0.33
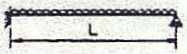	Elastic Elasto-Plastic Plastic	0.58 0.64 0.50	0.45 0.50 0.33	0.78 0.78 0.66
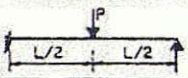	Elastic Elasto-Plastic Plastic	1.0 1.0 1.0	0.43 0.49 0.33	0.43 0.49 0.33
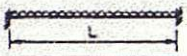	Elastic Elasto Plastic Plastic	0.53 0.64 0.50	0.41 0.50 0.33	0.77 0.78 0.66
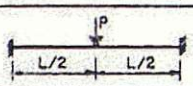	Elastic Plastic	1.0 1.0	0.37 0.33	0.37 0.33
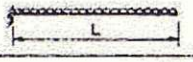	Elastic Plastic	0.40 0.50	0.26 0.33	0.65 0.66
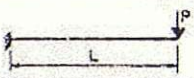	Elastic Plastic	1.0 1.0	0.24 0.33	0.24 0.33
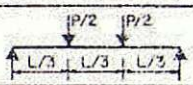	Elastic Plastic	0.87 1.0	0.52 0.56	0.60 0.56

Figure 1-3: Transformation factors for one-way elements from Table 3-12 of TM5-1300 (1990)

B1.3.1 Numerical solution or constant-velocity method

Numerical methods are used to allow the response of the system to be analysed at each time step as the loading is applied. The process starts at time equals zero, where the initial conditions are known, and solves the equation of motion step by step for discrete time intervals. The method assumes that between discrete time periods the velocity is constant (see Figure 1-4) and hence has become commonly known as the constant-velocity method. The displacements, u_s and u_{s-1}, at time

periods *s* and *s-1* respectively are used to calculate the acceleration at time s using the equation of motion. The next stage is to determine the displacement at time *s+1* using extrapolation.

$$u_{s+1} = u_s + \dot{u}_{av}\Delta t \qquad \text{B26.}$$

Where $\dot{u}_{av}$ is the average velocity between time periods *s* and *s+1*. The average velocity is simply:

$$\dot{u}_{av} = \frac{u_s - u_{s-1}}{\Delta t} + \ddot{u}_s \Delta t \qquad \text{B27.}$$

This is found by assuming that $\ddot{u}_s$ is an average acceleration throughout the time period. This is equivalent to approximating the acceleration time curve to a series of straight lines as shown in Figure 1-4.

Substitution of Eqn 3.27 into Eqn 3.26 gives:

$$u_{s+1} = 2u_s - u_{s-1} + \ddot{u}_s(\Delta t)^2 \qquad \text{B28.}$$

This allows the displacement at the next time step to be calculated.

The accuracy of the calculation is limited by the time interval, Δt, being kept small in comparison to the rate of change of acceleration. Biggs (1964) states that accurate results can be achieved by keeping the time interval smaller than 1/10 of the natural period of vibration of the system.

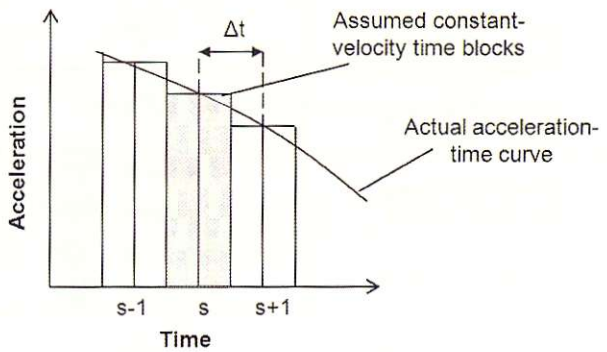

Figure 1-4: Constant-velocity procedure

The displacements can then be found for each time step starting at time t = 0. However a problem arises in the first time period in that the previous displacement is unknown. It is therefore assumed the acceleration is constant during the first time interval. This makes the displacement, for the first time period only:

$$u_{s+1} = \frac{1}{2}\ddot{u}_s(\Delta t)^2 \qquad \text{B29.}$$

The equation of motion is thus solved using a spreadsheet and for each successive time period the displacement is calculated.

The advantage of this method is that the displacement of the lumped-mass is calculated at each discreet time step. When all of these displacements are plotted on the same graph, the overall displacement-time history is depicted.

The general properties of a single degree system are given by:

$$\text{Natural angular frequency: } \omega_n = \sqrt{\frac{k}{M}}$$

$$\text{Natural time period: } T = \frac{2\pi}{\omega_n} = 2\pi\sqrt{\frac{M}{k}} \qquad \text{B30.}$$

$$\text{Natural frequency: } f = \frac{\omega_n}{2\pi} = \frac{1}{T}$$

B1.4 Bending moments and shear forces

For simply supported beams with a distributed load, TM5-1300 guidance includes the method to calculate the maximum support shear using:

$$\text{Maximum Shear} = \frac{\text{Maximum resistance*Length}}{2}$$

The maximum resistance is calculated from the ultimate resistance of the beam. Formula for alternative support and loading conditions are shown in Figure 1-5.

Edge Conditions and Loading Diagrams	Support Reactions, V_s
L	$\frac{r_u L}{2}$
P; L/2, L/2	$\frac{R_u}{2}$
L	L. Reaction $\frac{5 r_u L}{8}$ R. Reaction $\frac{3 r_u L}{8}$
P; L/2, L/2	L. Reaction $\frac{11 R_u}{16}$ R. Reaction $\frac{5 R_u}{16}$
L	$\frac{r_u L}{2}$
P; L/2, L/2	$\frac{R_u}{2}$
L	$r_u L$
P; L	R_u
P/2, P/2; L/3, L/3, L/3	$\frac{R_u}{2}$

Figure 1-5: Calculating support shear for one-way elements from Table 3-9 of TM5-1300 (1990)

An alternative method to calculate the shear force is to use the dynamic reactions method where the analysis includes the inertia forces of the beam upon deflection. The free body diagram of a beam subjected to dynamic loading is given in Figure 1-6.

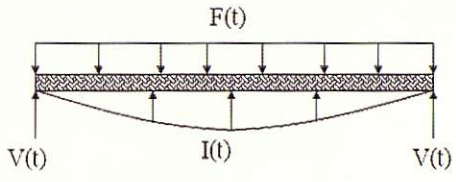

Figure 1-6: Free body diagram of dynamic problem

The distribution of the inertia force acting on the beam, *I(t)*, is identical to the deflected shape due to the motion being harmonic. The dynamic reactions acting at the supports, *V(t)*, depend upon both the load, *F(t)*, and the inertia force.

A convenient way of calculating the dynamic reactions can be achieved by considering one half of the beam as shown in Figure 1-7. From symmetry the shear force at midspan, S, equals zero.

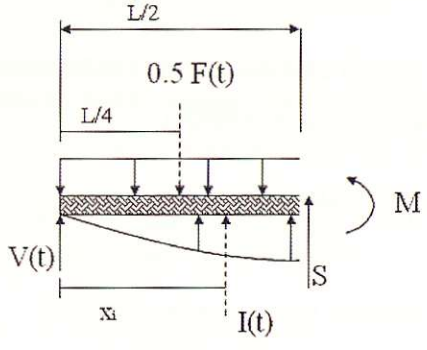

Figure 1-7: Determination of dynamic reactions

The centroid of the inertia force acts at a distance x_i from the left hand support. The total moment of area equals the sum of all the individual moment of areas this can be rearranged to find the point at which the moment area acts, where u is a function of x defined by the deflected shape.

$$x_i \int_0^{L/2} u \cdot dx = \int_0^{L/2} ux \cdot dx \qquad \text{B31.}$$

$$x_i = \frac{\int_0^{L/2} ux \cdot dx}{\int_0^{L/2} u \cdot dx} \qquad \text{B32.}$$

The deflected shape assumed will thus alter the position about which the centroid of the inertia force acts.

Once the point at which the inertia force acts has been found it is possible to take moments about this point thus obtaining:

$$V(t)x_i - M_{mid} - \frac{F(t)}{2}\left(x_i - \frac{L}{4}\right) = 0 \qquad \text{B33.}$$

The bending moment at midspan (M_{mid}) is calculated from the deflected shape using the engineers bending formula:

$$M = \frac{\delta^2 u}{\delta x^2} EI \qquad \text{B34.}$$

Rearranging Eqn 3.33 and substituting for *M* gives:

$$V(t) = \frac{1}{x_i}\left(M_{mid} - \frac{F(t)L}{8}\right) + \frac{F(t)}{2} \qquad \text{B35.}$$

This is a general formula to calculate the dynamic support shear force for any assumed deflected shape.

B1.4.1 Elastic behaviour

The shape functions most often used in analysis are the fundamental mode or the equivalent static deflected shape given below [Baker, Cox et al. (1983)].

$$u(x) = \frac{16u_{max}}{5L^4}(x^4 - 2Lx^3 + L^3x) \qquad \text{B36.}$$

The point where the inertia force acts, x_i, is found using Eqn 3.32:

$$x_i = \frac{\int_0^{L/2}\left[\frac{16u_{max}}{5L^4}(x^4 - 2Lx^3 + L^3x)\right] x \cdot dx}{\int_0^{L/2}\frac{16u_{max}}{5L^4}(x^4 - 2Lx^3 + L^3x) \cdot dx} \qquad \text{B37.}$$

Solving this gives:

$$x_i = \frac{61L}{192} \qquad \text{B38.}$$

From Eqn 3.36 it is calculated that:

$$\frac{\delta^2 u}{\delta x^2} = \frac{16u_{max}(-12Lx + 12x^2)}{5L^4} \qquad \text{B39.}$$

Substitution from Eqn 3.34, the bending moment at midspan ($x=L/2$) is therefore:

$$M_{mid} = \frac{48u_{max}}{5L^2} EI \qquad \text{B40.}$$

Equating Equations B35, B36, B38 and B40 provides:

$$V(t) = 0.1066F(t) + \frac{30.216u_{max}}{L^3}EI \qquad \text{B41.}$$

This can be used to calculate the equivalent support reactions throughout the analysis procedure.

An alternative shape function is the first mode of vibration:

$$u(x) = u_{max}\sin\left(\frac{\pi x}{L}\right) \qquad \text{B42.}$$

The same method is used to calculate the location of the inertia forces and it can be shown that x_i is $\frac{L}{\pi}$. Similarly the midspan moment is $\frac{EI\pi^2 u_{max}}{L^2}$. Substituting these values into Equation B31 gives the dynamic reactions as:

$$V(t) = \frac{EI\pi^3 u_{max}}{L^3} + F(t)\left(0.5 - \frac{\pi}{8}\right)$$
$$= 0.1073F(t) + \frac{31.006u_{max}}{L^3}EI \qquad \text{B43.}$$

The dynamic reactions of a typical SDOF system were analysed using the two shape functions outlined above. The results are plotted on the same axes and are shown in Figure 1-8. These results show that the two shape functions produce similar dynamic reactions but that using a sine curve predicts slightly higher peak values (less than 1% difference).

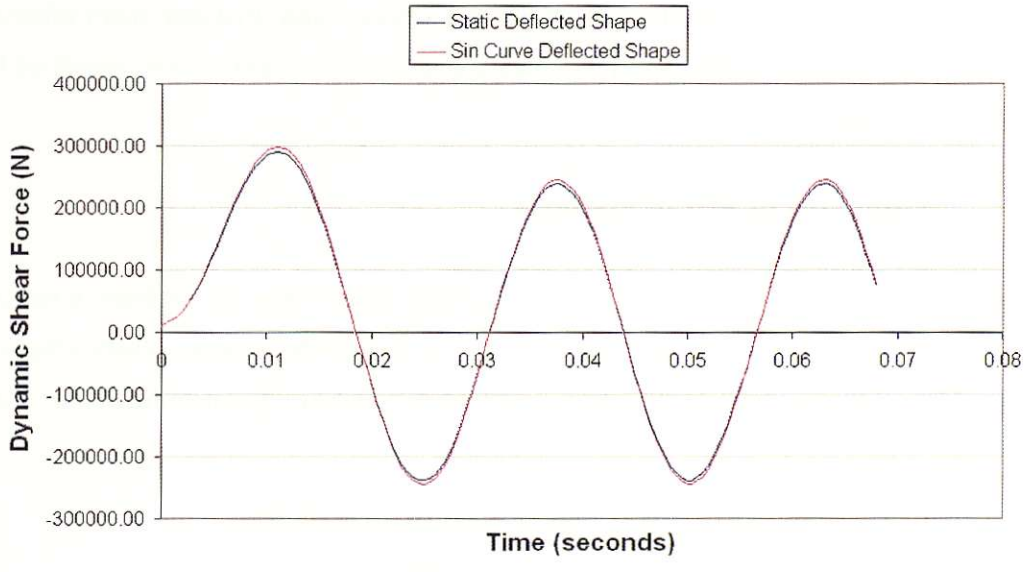

Figure 1-8: Comparison of dynamic reactions using sin curve and static deflected shape

A similar comparison has been conducted for the midspan bending moments and once again the sine curve produces a slightly higher peak.

It must be noted that neither of these functions may be suitable assumptions under blast loading. This is especially the case for strong, short duration loading where high curvature may expected at the supports producing much higher shear forces.

B1.4.2 Plastic behaviour

Equations B35 and B37 were calculated for elastic behaviour. If yielding occurs before the maximum load, then the beam plastic moment, M_p, replaces the midspan moment in the equations. For the first mode of vibration (Eqn B43) V becomes:

$$V(t) = 0.1073F(t) + \frac{192M_p}{61L} \qquad \text{B44.}$$

Further, the plastic moment can be expressed in terms of the maximum resistance, R_m, defined as the magnitude of the static load necessary to cause a plastic hinge at the center of the beam, Smith and Hetherington (1994).

$$R_m = \frac{8M_p}{L} \qquad \text{B45.}$$

Thus Eqn. B44 can be expressed in the form:

$$V(t) = 0.1073F(t) + \frac{24}{61}R_m \approx 0.11F(t) + 0.39R_m \qquad \text{B46.}$$

Eqn. 3.46 is of the form given in Smith and Hetherington (1994) Table 10.2 and many other texts on blast loading. A difference of less than 1% is obtained when the coefficients are calculated from the static deflected shape.

B1.5 Summary of SDOF methods

Single degree of freedom systems have been used for a long time to allow the analysis of structural elements under dynamic conditions and have been shown to provide accurate results [Naito and Wheaton (2006)] as long as certain criteria are met in the analysis. Limitations of the method include:

- End condition assumptions must be made (rigid or simple).
- Local deformations of model are not possible.
- Non-symmetrical loading conditions are not accounted for.
- Whilst the method was developed to predict the correct midspan deflection, the corresponding bending moments and shear forces are calculated from the assumed deflected shape which is not always the same as the static deflected shape. This can lead to gross underestimations of loading at the support conditions as

Paramasivam (2008) found. Alternative deflected shapes can be used but these must be verified experimentally.

Taking into account these limitations, SDOF systems are useful in providing a quick method of analysis however a more detailed methodology which can improve upon these limitations is sought.